國立交通大學

應用化學研究所

碩士論文

雙芘取代的多面體聚矽氧烷複合奈米粒子:探討其晶體的微結構以及光致發光的應用

Bispyrenyl POSS Nanoparticle Hybrids: Crystal Microstructures and Applications

研究生：蔡佳樺

指導教授：張豐志 教授

中華民國九十八年六月

誌謝

驪歌輕唱，轉眼間我已完成碩士學業，一路從交大應化的大學部念到碩士畢業，已經過了六年的時間，這段學習的過程對我來說是很寶貴的經驗。

在我碩士研究生涯裡，首先我要感謝我的指導教授張豐志老師，感謝老師給我機會在大二的時候就進實驗是做專題，老師強調的自動自發，讓我可以自由的發揮，培養出自己對研究的興趣。其次我要感謝我的口試委員，台科大陳建光教授和中山大學郭紹偉教授，給予本論文的建議與指導，讓本論文更臻完備。另外我要感謝小杜學長，在我做專題的時候教導我實驗的方法和技巧，才能讓我在實驗上更順利。在實驗上我要感謝didi學長、智嘉學長、英傑學長以及昀昇學長，有你們在實驗上的指點和帶領讓我能有今日的成果。

此外要感謝世堅(你亢)、阿發學長們，感謝你們對實驗室辛苦的付出，以及宜弘、狗弟、文騰、筱雯，感謝你們不僅在實驗上也在生活上的幫忙，接著要感謝小朱、業昇，你們是我最好的球友，以及實驗室學弟妹耀正、嘉蔚、佳佑、雅萍、郁娟、昶禎，讓我有志同道合的朋友，有你們這些同學及學弟妹的陪伴，使我碩士生活更加快樂。另外我要感謝一直陪在我身邊的幼幼社朋友們，bug、阿寬、云琦、豪哥、如屏和白兔，在我心情低落的時候，你們的笑容是最好的解藥。

最後我要感謝我的家人，有你們在我背後的支持，才能讓我可以順利完成碩士學業，在你們的鼓勵下，我也會繼續努力來達成之後的目標。

佳樺　2009 年 6 月

Outline of Contents

Pages

List of Tables

Pages

List of Schemes

List of Figures

雙芘取代的多面體聚矽氧烷複合奈米粒子:探討其晶體的微結構以及光致發光的應用

學生：蔡佳樺　　指導教授：張豐志

國立交通大學應用化學研究所　碩士班

摘　　要

我們利用零價鉑催化的氫化反應使含有矽烷官能基的異丁基多面體聚矽氧烷與含有雙芘取代的雙鍵分子反應而合成出一個單官能基雙芘取代的異丁基多面體聚矽氧烷(蝴蝶狀的BPy-POSS).我們對BPy-POSS的性質做了一連串的研究.從微分掃描卡計 (DSC)中我們可以發現BPy-POSS是一個像高分子一樣,半結晶性的小分子,在放射光譜中也可看出芘類強烈的excimer emission.我們製備出混合不同比例的BPy-POSS和i-Bu POSS的薄膜,並且探討它們的微結構. 經由光學顯微鏡以及原子力顯微鏡,我們觀察出其特殊的蕨葉狀微結構;我們猜想此一蕨葉狀微結構的形成是由於i-Bu POSS和i-Bu POSS 的堆疊.在溶劑揮發到結晶的過程,i-Bu POSS會先結晶作為一個 POSS 的基板,然後BPy-POSS再分散在i-Bu POSS基板的表面上.使用X-ray 散射圖譜以及微分掃描卡計我們也確實可以證明i-Bu POSS和BPy-POSS

會微觀相分離的結果.我們利用這種會自組裝的特點形成雙芘的薄膜可應用在硝基芳烴的氣體的偵測.當表面的雙芘暴露在充滿硝基芳烴的蒸氣裡,硝基芳烴很快速了抑制雙芘excimer emission.利用BPy-POSS和i-Bu POSS的自組裝薄膜, 使用少量的BPy-POSS也可以達到不錯的偵測效果.

Bispyrenyl POSS Nanoparticle Hybrids: Crystal Microstructures and Applications

Student：Chia-hua Tsai　　Advisors：Dr. Feng-Chih Chang

Institute of Applied Chemistry
National Chiao Tung University

ABSTRACT

A bispyrenyl monofunctionalized isobutyl-polyhedral oligomeric silsesquioxane (butterfly-like BPy-POSS) is synthesized by Pt (0)-catalyzed hydrosilylation between silane-monofunctional isobutyl-POSS and bispyrenyl alkene. By DSC, we found that BPy-POSS is a polymer-like semi-crystal molecule. Strong excimer emission was observed in PL spectra. Blends of BPy-POSS and isobutyl-POSS were fabricated to investigate their microstructures. Fern-like microstructures can be seen by OM and AFM; we suspected that the cause of forming fern-like structures is POSS-POSS recognition. During solvent evaporation, i-Bu POSS crystallize as a POSS template, and then BPy-POSS dispersed on the surface of POSS template. The data of XRD and DSC could be an evidence of phase separation of i-Bu POSS and BPy-POSS.

We used these self-assembled films to do the application of attachment to nitroaromatic compounds. Upon exposure to nitrobenzene vapor, the films show fast fluorescence quenching. The high performance is based on the microstructure of BPy-POSS and i-Bu POSS on the film surface. Using the self-assembled blend thin films of i-Bu POSS and BPy-POSS, we could achieve the goal of detection of nitrobenzene by using small amount of BPy-POSS.

Chapter 1

Introduction

1.1 Organic-Inorganic Hybrid Materials

1.1.1 Development of Organic-Inorganic Hybrid Materials

Thousands of years ago, the production of bright and colorful paints was the driving force to consistently try novel mixtures of organic dyes or inorganic pigments and other inorganic and organic components to form paints that were used thousands of years ago. Therefore, hybrid materials or even nanotechnology is not an invention of the last decade but was developed a long time ago. However, it was only at the end of the 20th and the beginning of the 21st century that it was realized by scientists. Apart from the use of inorganic materials as fillers for organic polymers, such as rubber, it was a long time before much scientific activity was devoted to mixtures of inorganic and organic materials. One process changed this situation: the sol-gel process. This process was developed in the 1930s using silicon alkoxides as precursors from which silica was produced. Contrary to many other procedures used in the production of inorganic materials this is one of the first processes where ambient conditions were applied to produce ceramics. The control over the preparation of multicomponent systems by a mild reaction method also led to industrial interest in that process. In particular the silicon based sol-gel process was one of the major driving forces what has become the broad field of inorganic-organic hybrid materials. Some similarities to sol-gel chemistry are shown by the stable metal sols and colloids, such as gold colloids, developed hundreds of years ago. Such metal colloids have been used for optical applications in nanocomposites for centuries. In particular many reports of the scientific examination of gold colloids, often prepared by reduction of gold salts, are known from the end of the 18th century. Probably the

first nanocomposites were produced in the middle of the 19th century when gold salts were reduced in the presence of gum arabic. Currently many of the colloidal systems already known are being reinvestigated by modern instrumental techniques to get new insights into the origin of the specific chemistry and physics behind this materials.[1]

1.1.2 Definition of Hybrid Organic－Inorganic materials

The term hybrid material is used for many different systems spanning a wide area of different materials, such as crystalline highly ordered coordination polymers, amorphous sol-gel compounds, materials with and without interactions between the inorganic and organic units. Hybrid organic-inorganic materials are not simply physical mixtures. The most wide-ranging definition is the following: A hybrid material is a material that includes two moieties blended on the molecular scale; commonly one of these compounds is inorganic and the other one organic in nature. A more detailed definition distinguishes between the possible interactions connecting the inorganic and organic species. For example there are hydrogen bonds that are definitely stronger than for example weak coordinative bonds (**Figure 1-1**).[1] Consequently the properties of hybrid materials are not only the sum of the individual contributions of both phases, but the role of their inner interfaces could be predominant. The nature of the interfaces has been used to grossly divide these materials into two distinct classes: (Sanchez 1994 New Journal of Chemistry) In Class Ⅰ, organic and inorganic components are embedded and only hydrogen, van der Waals or ionic bonds given cohesion to the whole structure. In Class Ⅱ materials, the two phases are partly linked together through strong chemical covalent or ionic-covalent bonds.[2]

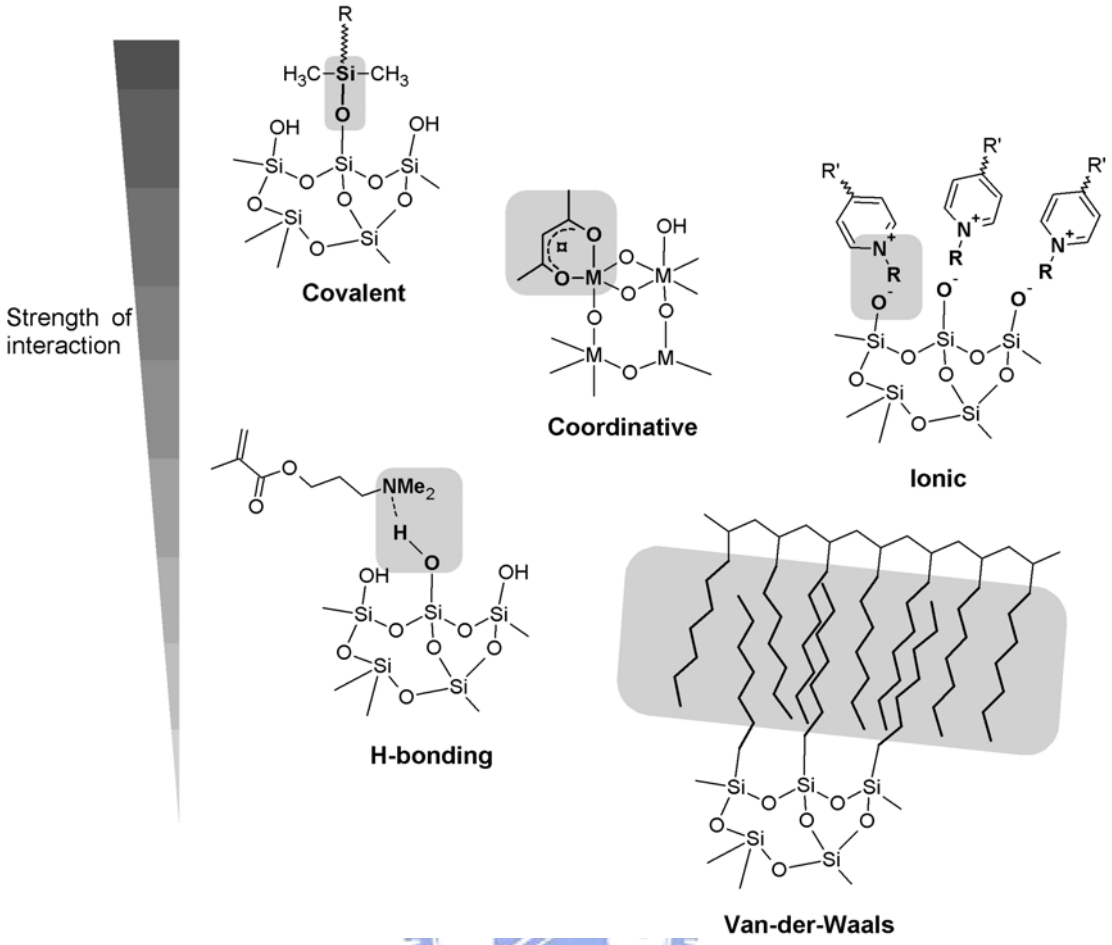

Figure 1-1. Specific interactions typically applied in hybrid materials and their relative strength.

1.1.3 Synthesis of hybrid materials

1.1.3.1 Sol-Gel Process

This process is chemically related to an organic polycondensation reaction in which small molecules form polymeric structures by the loss of substituents. The silicon-based sol-gel process is probably the one that has been most investigated; therefore the fundamental reaction principles are discussed using this process as a model system. One important fact also makes the silicon-based sol-gel processes a predominant process in the formation of hybrid materials, which is the simple incorporation of organic groups using organically modified silanes. Si-C bonds have

enhanced stability against hydrolysis in the aqueous media usually used, so it is possible to easily incorporate a large variety of organic groups in the network formed. Principally $R_{4-n}SiX_n$ compounds (n = 1-4, X = OR', halogen) are used as molecular precursors, in which the Si-X bond is labile towards hydrolysis reactions forming unstable silanols (Si-OH) that condensate leading to Si-O-Si bonds. In the first steps of this reaction oligomers and polymers as well as cyclics are formed subsequently resulting in colloids that define the sol. Solid particles in the sol afterwards undergo crosslinking reactions and form the gel (**Scheme 1-1**).[1]

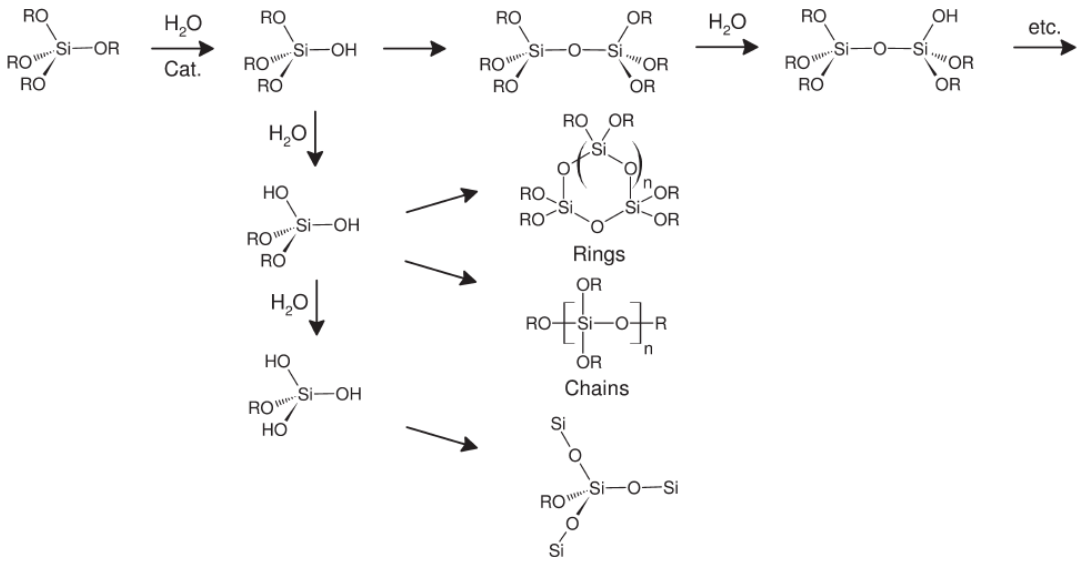

Scheme 1-1. Typical sol-gel process using tetrialkoxysilanes.

1.1.3.2 Hydrosilylation

The hydrosilylation reaction is a general method of adding a Si-H bond across a C-C double bond. This method encompasses a wide variety of substituted alkenes, dienes, and alkynes leading to many different organosilicon products.[3] Trialkoxysilane groups are typically introduced by a platinum catalyzed reaction between an unsaturated bond and a trialkoxysilane (**Scheme 1-2**).[1] The mechanism is usually assumes the

intermediacy of a metal complex that contains a hydride, a silyl ligand (R_3Si), and the alkene or alkyne substrate (**Scheme 1-3**).[4-5] In our research, we used the Karstedt's catalyst to complete the hydrosilylation (**Scheme 1-4**).[6]

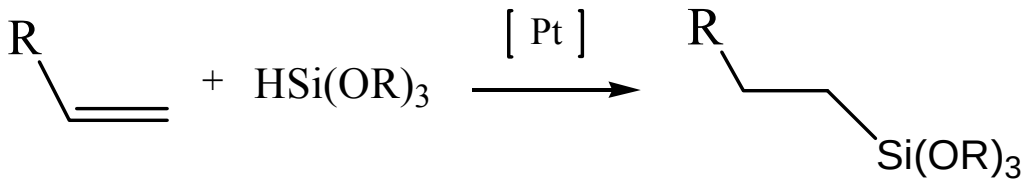

Scheme 1-2. Pt(0)-catalyzed hydrosilylation.

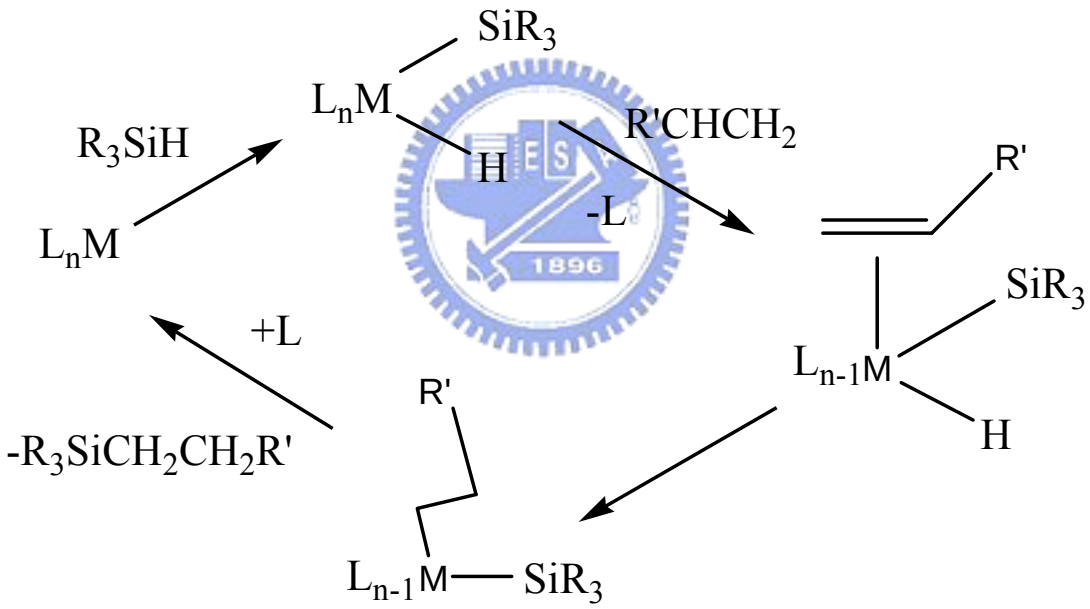

Scheme 1-3. Metal-catalyzed hydrosilylation of an alkene.

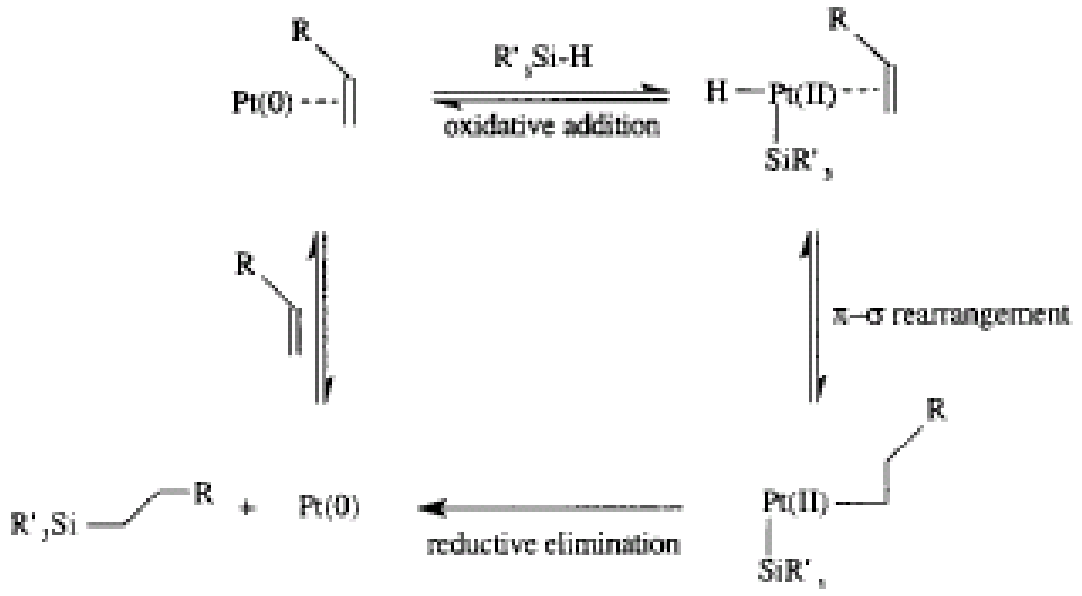

Scheme 1-4. Mechanism of hydrosilylation using a Karstedt's catalyst.

1.1.4 Application of hybrid materials

Organic-inorganic hybrids can be applied in many branches of materials chemistry because they are simple to process and are amenable to design on the molecular scale. Organic-inorganic hybrid materials do not only represent a creative alternative for the design of new materials and compounds for academic research, but their improved or unusual features open promising applications in many areas: optics, electronics, ionics, mechanics, energy, environment, biology and medicine. Applications include smart membranes and separation devices, functional smart coatings, a new generation of photovoltaic and fuel cells, photocatalysts, new catalysts, sensors, smart microelectronics, micro-optical and photonic components and systems for nanophotonics, innovative cosmetics, intelligent therapeutic vectors that combine targeting, imaging, therapy and controlled release of active molecules, nanoceramic-polymer, composites for the automobile or packaging industries, etc…

1.2 Polyhedral Oligomeric Silsesquioxanes (POSS)

1.2.1 Development of POSS

Earliest in 1900s, Silsesquioxanes was obtained by Kipping using hydrolysis and polycondensation of silane compounds,[7] but it wasn't complete; until 1960s, Brown and Vogt build up a more complete method of synthesis of silsesquioxanes.[8] In 1994, for development of one kind of polymer material with light and high performance, US Airforce Research Laboratory chose the PDMS (polydimethylsiloxane), designed and produced on large scale of a series of polyhedral oligomeric silsesquioxanes (POSS).

1.2.2 Structure and Special Properties of POSS

Silsesquioxanes are products of sol-gel reactions between monofunctional trichloro-silanes and trialkoxy-silanes nanostructures; they have the chemical structure $(RSiO_{1.5})_n$, where R is a hydrogen atom or an organic functional group, such as an alkyl, alkylene, acrylate, hydroxyl, or epoxide unit, and n is the number of repeating units. **Figure 1-2** indicates that silsesquioxanes may be formed in random, ladder, cage, and partial-cage structures. The siloxane plane having the chemical structure $Si_4O_4R_4(OH)_4$ is the building block in the ladder polysilsesquioxanes and the cage-type polyhedral oligomeric silsesquioxane (POSS) derivatives. Interestingly, POSS molecules can be regarded as cyclic polysilsesquioxane oligomers; for example, T8, T10, and T12 POSS are cyclic oligomers with 4, 5, and 6 planes of $R_4Si_4O_4$ units. (T = number of $RSiO_{1.5}$ units; **Fig. 1-2b, c**).[9] Recent years, research of POSS focuses on the T8 shape; T8-POSS is a cage-like structure, instead of a cube structure (**Figure 1-3**). In 1957, K. Olsson[10] used X-Ray to characterize the structure of POSS, in his research, it could be seen that the cage-like structure is not symmetrical; the average angle of Si-O-Si is 145°, and angles of O-Si-O is in the range of 108-113°; the average value of bond length is 1.61±0.025 Å (**Figure 1-4**). POSS are completely defined

molecules of nanoscale dimensions that may be functionalized with reactive groups suitable for the synthesis of new organic-inorganic hybrids, thus providing the opportunity to design and build materials with extremely well-defined dimensions possessing nanophase behavior.[9,11-24]

Highly symmetric T8-POSSs with alkyl chains on a siloxane cube can pack into a crystal with hexagonal unit cells expect for hydrosilylated amorphous T8-POSS products (a mixture of α- and β-isomers). [9,14] Due to freely intramolecular rotation, the monofunctional T8-POSSs, sol-gel products between trisilanol T7-POSS and mono-functional silane, can be also served as spheres to form a similar crystal.[15] POSS molecules can be regarded as core-shell colloids with solvated alkyl or aryl shells to disperse insoluble siloxane cores in solution. Thus, POSS crystals should be modeled upon the molecular packing of soft balls on a given substrate in comparison with hard spherical models for metal crystals.

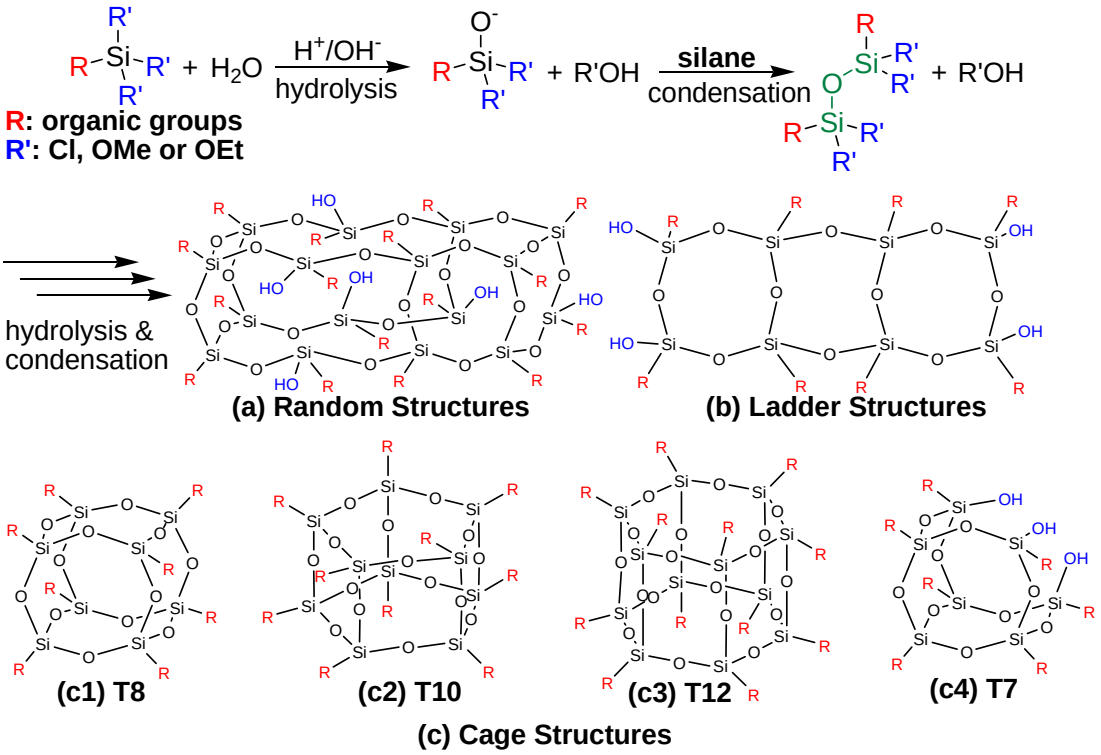

Figure 1-2. Preparation and chemical structures of silsesquioxanes $(RSiO1.5)_n$: (a) random networks, (b) ladder chains, and (c) the cage NPs T8 (n = 8), T10 (n = 10), T12 (n = 12), and T7 (n = 7).[11]

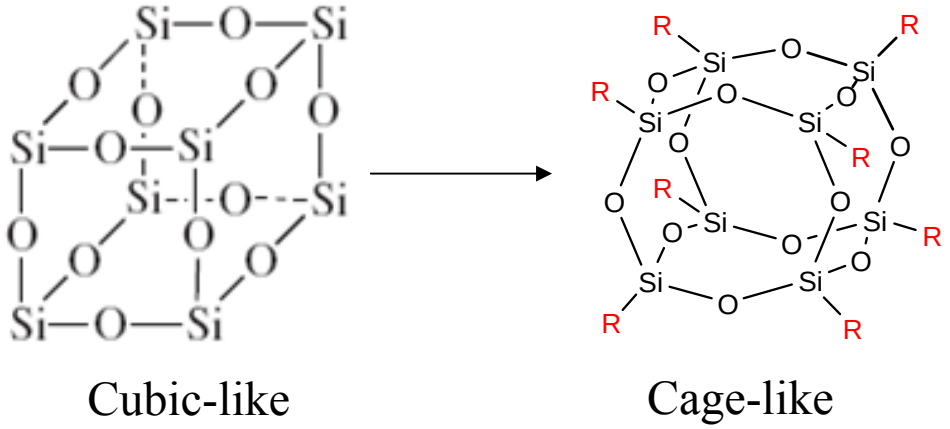

Figure 1-3. Cube and cage-like structure of POSS.

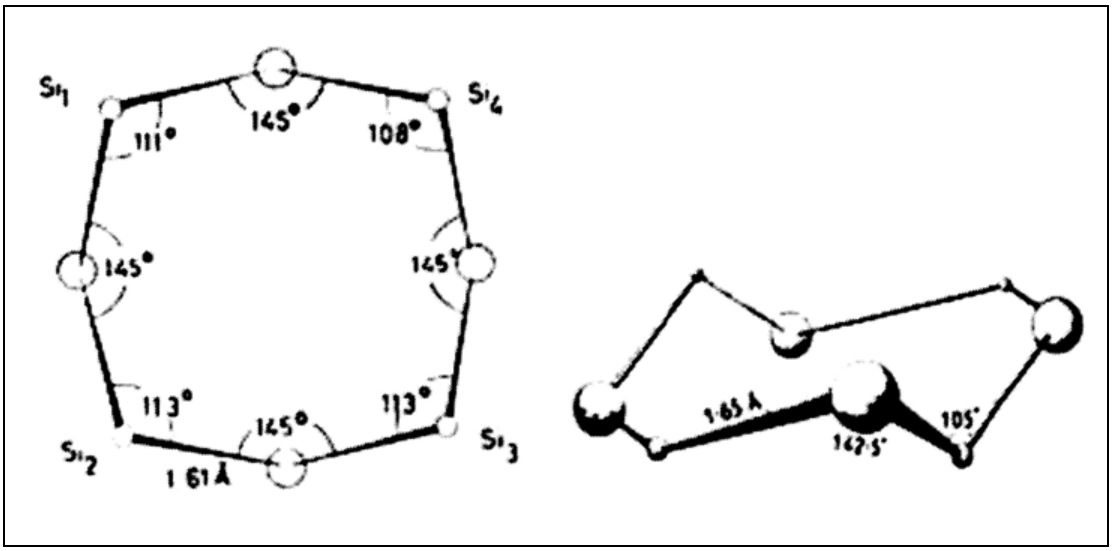

Figure 1-4. Theoretical bond angle and bond length of T8-POSS.

1.2.3 Synthesis of POSS

(a) Synthesis of POSS with partially condensed structure

POSS **2** and **3** in **Figure 1-5** are synthesized via the hydrolytic condensation of $RSiCl_3$ (R= *cyclo*-C_6H_{11}) in acetone at room temperature; the product yield depends on the reaction time and reached ~70%. The product is a readily resolvable mixture containing ~45% **3** and ~15% **2**.[8,25-26]

(b) Synthesis of monofunctional POSS with condensed structure

Monofunctional POSS are usually synthesized by a corner capping reaction of a trisilanol, $R_7Si_7O_9(OH)_3$, containing seven nonreactive organic groups such as *c*-C_5H_9, *c*-C_6H_{11}, and *i*-C_4H_9, with R'SiX_3, where R' bears a reactive site (vinyl, allyl, isocyanate, epoxy, etc.) and X = halogen or alkoxide (**Figure 1-6**).[27-29] The hydrosilylation reactions of unsaturated organic monomers with monofunctional silanes containing one reactive group X = H or $OSi(CH_3)_2H$ play an important role in the POSS functionalization processes. The reactions of hydrosilylation of unsaturated organic monomers with POSS **5** in the presence of 0.01-5 wt % Karstedt's or Speier's catalyst are used for preparation in a quantitative yield of mono-functionalized POSS

(**6**) or another POSS containing a *cyclo*-olefin group (R = *cyclo*-C_6H_{11} or *cyclo*-C_5H_9). (**Figure 1-7**).[25,30-31]

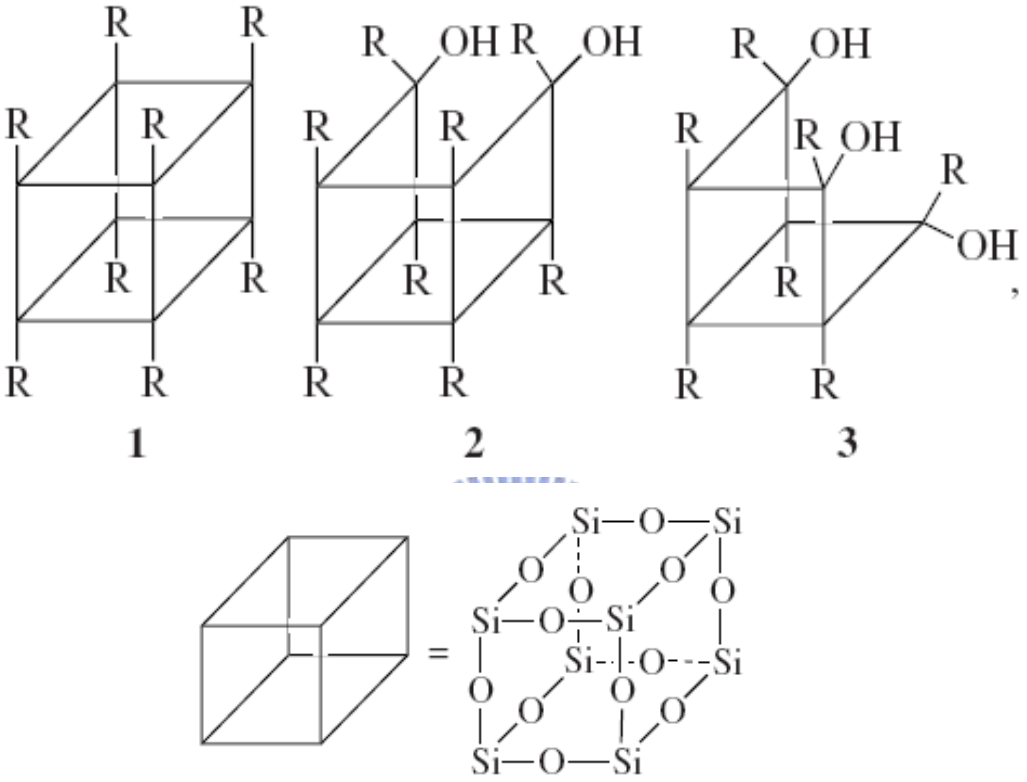

Figure 1-5. Completely (**1**) and partially (**2, 3**) condensed structures of POSS.

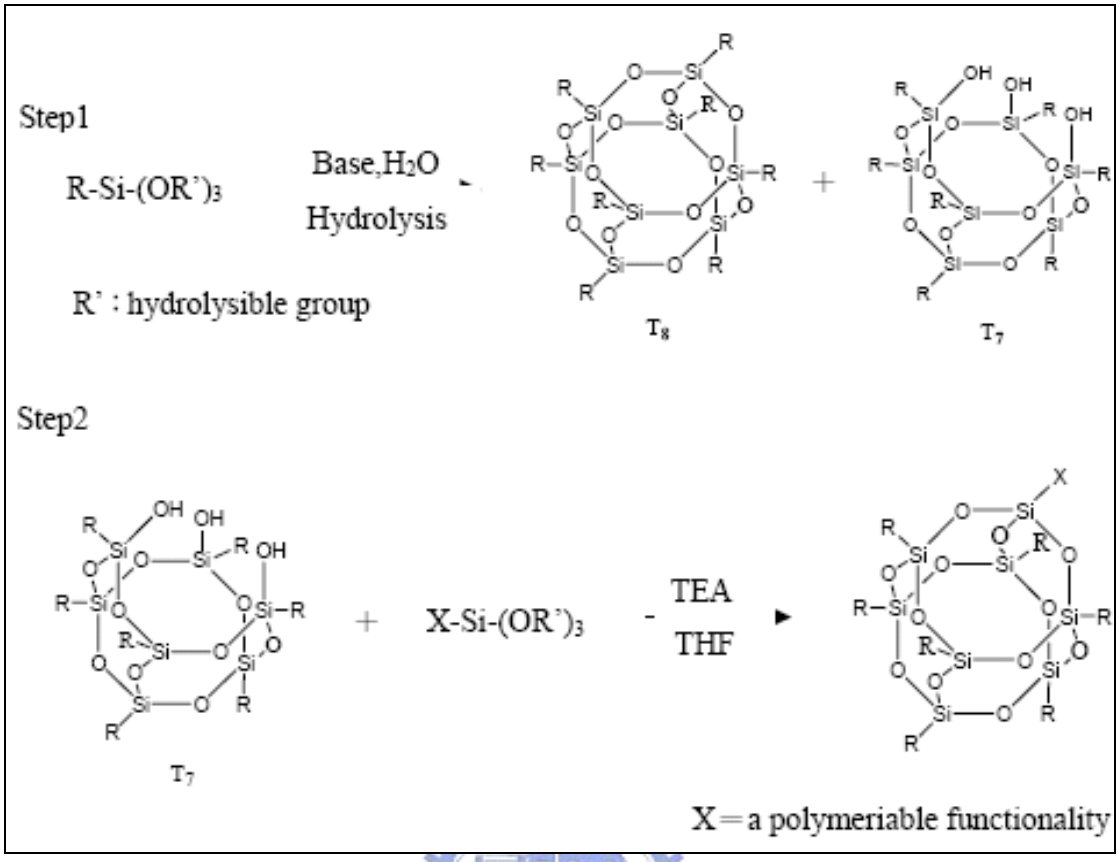

Figure 1-6. Synthesis of monofunctional POSS.

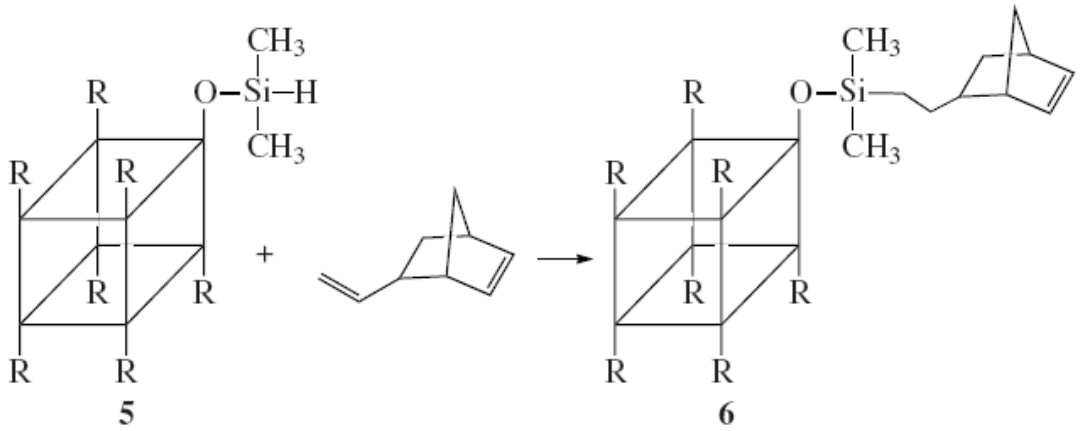

Figure 1-7. Monofunctionalized POSS prepared by hydrosilylation.

1.2.4 Microstructure of POSS

Self-assembly of functionalized nano-building blocks is a promising strategy for "bottom-up" materials design. Self-assembly of nanoparticles (NPs)-i.e., the

controlled organization of NPs into ordered or hierarchical structures allows coupling of their size- and shape-dependent properties to obtain potentially useful materials for optoelectronics, sensing, imaging, and biomedical applications.[32-35] A broad range of targeted self-assembled structures can be produced by organizing NPs exhibiting compositional heterogeneity.[36-39] They can be realized either by synthesizing NPs from several different materials or by selectively attaching organic molecules to different sites of the NPs.[40-42] Compositional heterogeneity makes NPs conceptually similar to amphiphilic molecules (e.g., surfactants or block copolymers) and allows the thermodynamic approach of self-assembly to be used to form "colloidal molecules" in energetically favorable structures possessing unique properties.[43-53] Ordered monolayers of NPs over large surface areas are sensitive to the presence of defects on the substrate's surface, which can destroy the assembly. In contrast, large ordered arrays of NPs can be obtained through judicious choice of the types of chemical interactions between the particles and the substrate.[54-55]

Platelike morphologies of POSS crystals, with lateral dimensions on the order of a few micrometers and thicknesses of a few hundred nanometers, have been described several times previously.[14,16] Waddon et al.,[16] indicated that the crystal structure and morphology of one specific POSS monomer with alkyl attachments was characterized using X-ray and electron microscopy method (**Figure 1-8** and **Figure 1-9**). The eight cornered central cages arrange in one plane on a hexagonal array. These cages can be regarded as being approximately spherical. The three-dimensional structure is achieved by stacking such hexagonally packed planes in ABCA sequence such that each fourth layer lies exactly above the first layer,[56] as shown schematically in **Figure 1-10**.[16] Lei Zhu' s group[17] investigated the self-assembly behavior of POSS linked with liquid crystal, an asymmetric disk-cube dyad molecule was synthesized by covalently attaching 2-hydroxy-3,6,7,10,11- pentakis(pentyloxy)triphenylene

(P5T-OH) discotic molecule to a cubic polyhedral oligomeric silsesquioxane (POSS) molecule via a spacer. The sample was denoted as P5T-POSS. The PLM observations of P5T-POSS at room temperature in **Figure 1-11** showed poorly organized crystalline spherulites. Because the isotropization of P5T liquid crystals and melting of POSS superposed at 66 °C in neat P5T-POSS, this micrograph represented a state where P5T was liquid crystalline and POSS was crystalline.[17]

In Lu's paper,[15] ordered fernlike 3D microstructures of assembled POSS-Au hybrid NPs onto a large-scale crystalline POSS template was prepared. The fernlike structure of the POSS-Au hybrids was analyzed using TEM and AFM (**Figure 1-12**), and they propose the structural model for the formation of the fernlike hybrid microstructures in **Figure 1-13**. During the process of solvent evaporation, excess SH-POSS colloids (i.e., those not bound onto Au cores) tend to pack in the form of fernlike and platelike crystals that function as templates for the self-assembly of POSS-Au NPs onto the surface interstices of the SH-POSS crystals. Upon reducing the SH-POSS concentration in toluene, the SH-POSS colloids on the second layer of the bilayer of the POSS-Au NPs are released to fill the gaps between the incorporated Au NPs. Finally, the monolayer-protected POSS-Au NPs aggregated at the boundaries of the fern micropatterns, resulting in the POSS-Au NP hybrid fernlike micropatterns. Thus, POSS hybrid nanoparticles would be excellent and functional building blocks for microsized and nanosized ordered patterns.

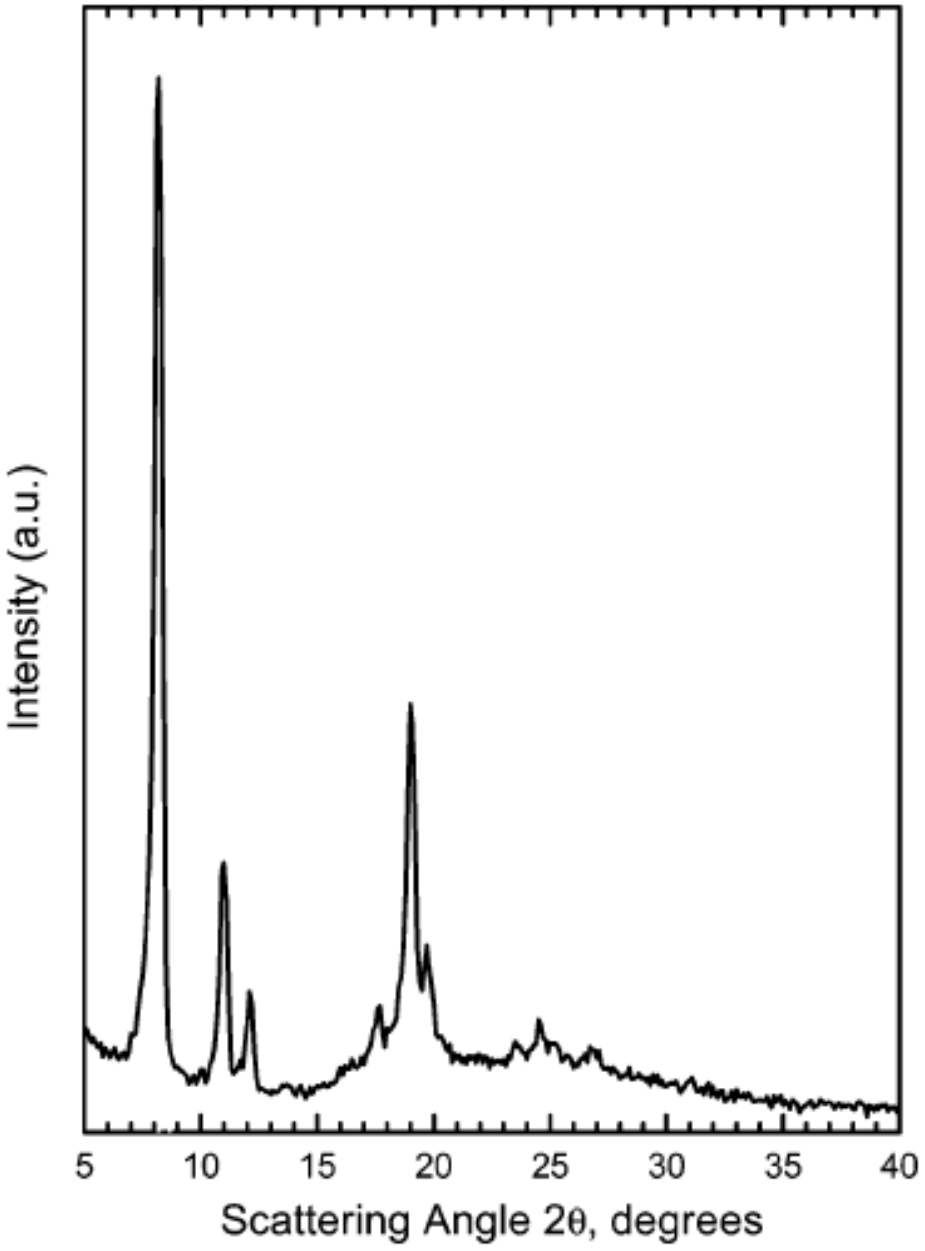

Figure 1-8. XRD spectrum of POSS cyclopentyl-norbornyl monomer.

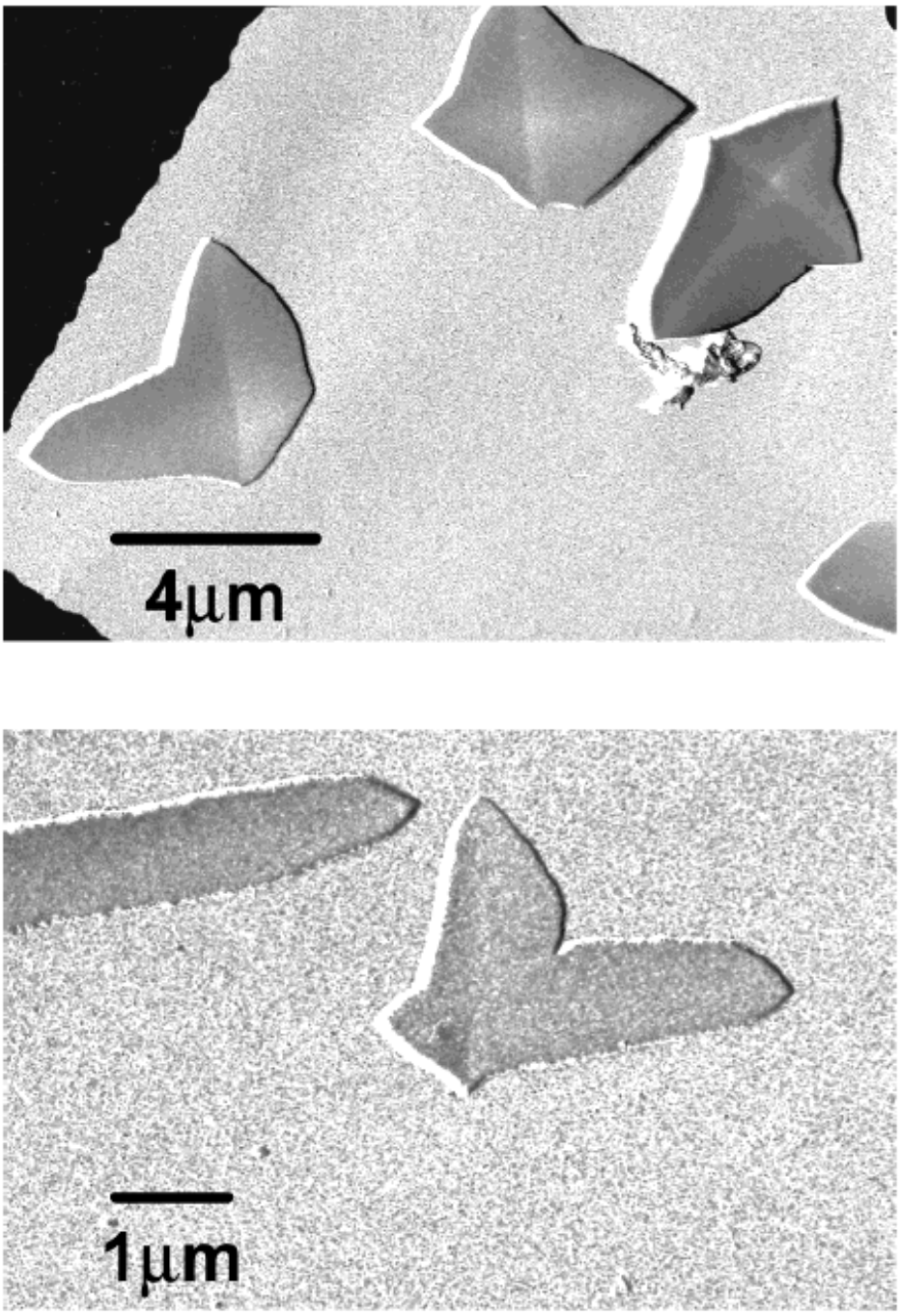

Figure 1-9. Transmission electron micrographs of crystals of cyclopentyl-norbornyl monomer (Gold shadowed).

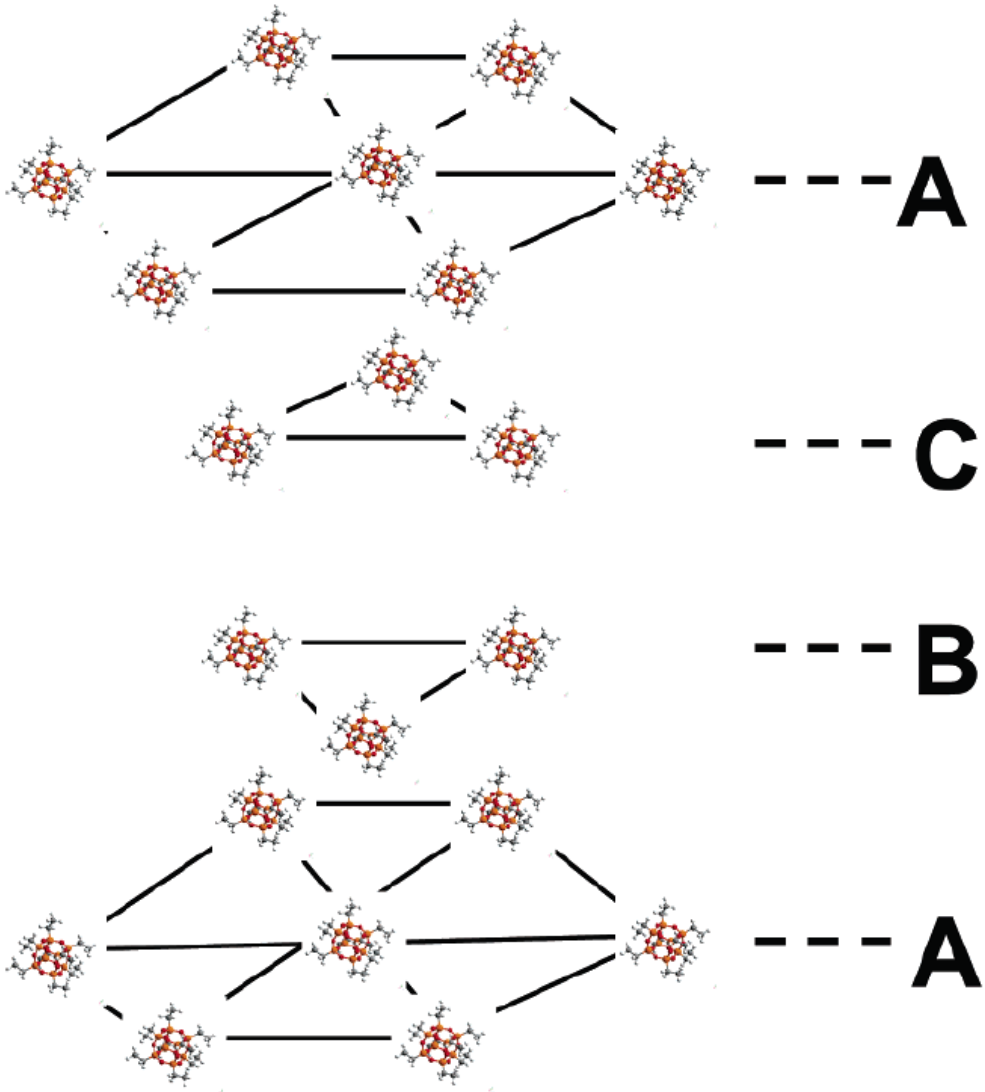

Figure 1-10. Schematic of hexagonally packed POSS molecules. The sequence of packing in adjacent layers is ABCA. This figure is purely schematic and the distances within the structure as drawn are not intended to be representative of the values in the real crystal.

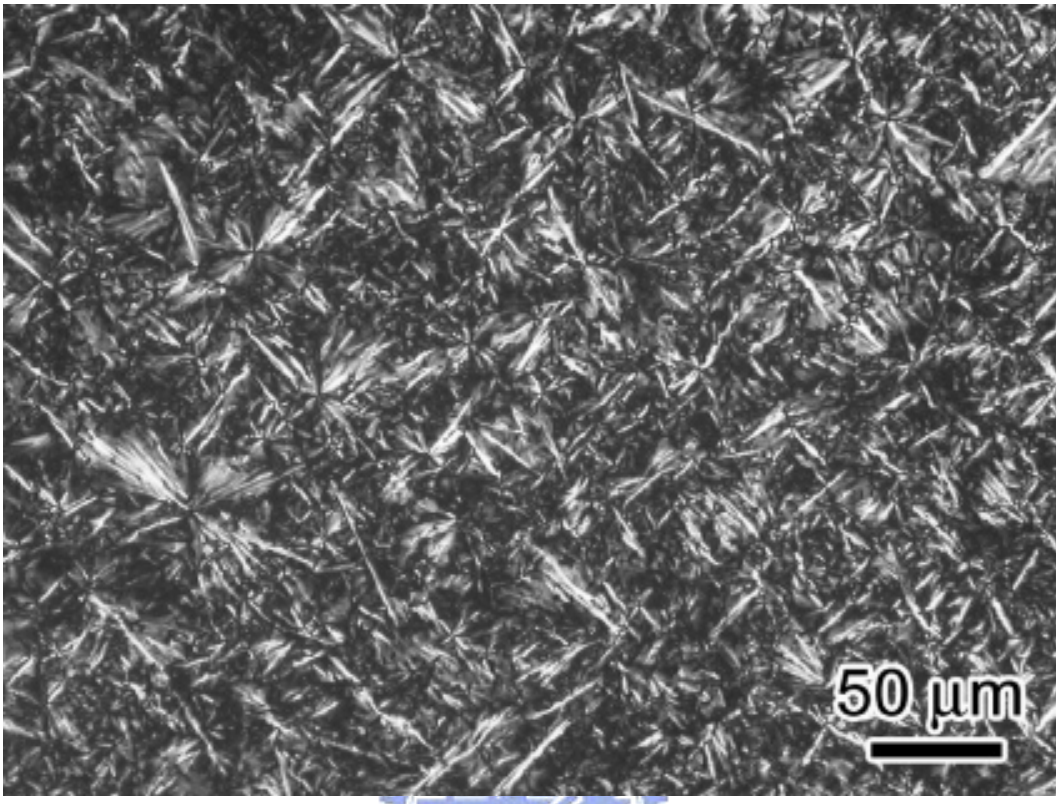

Figure 1-11. PLM micrograph of P5T-POSS at room temperature.

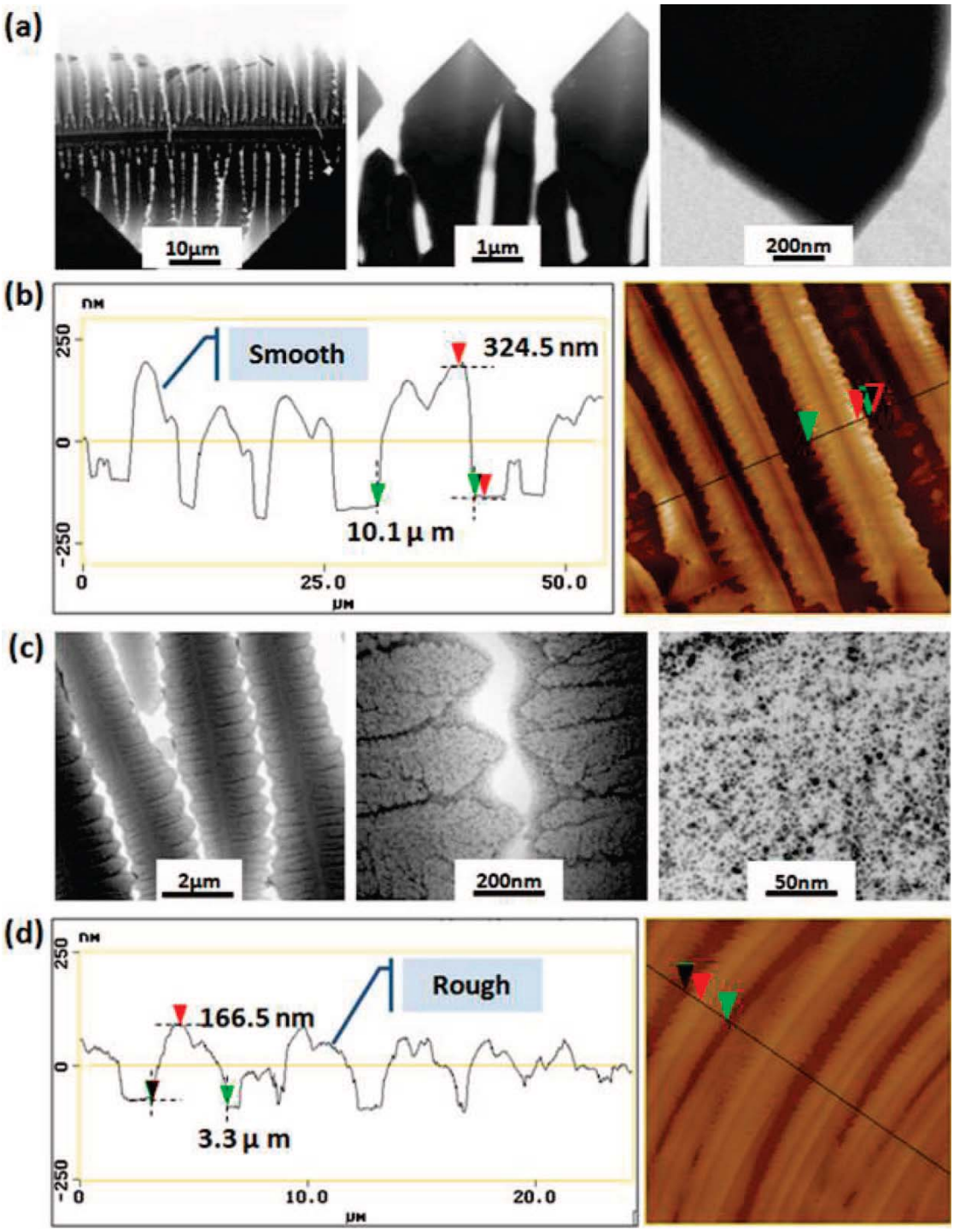

Figure 1-12. TEM images, (various) magnifications, and AFM sectional analyses of the (a, b) SH-POSS and (c, d) POSS-Au1 fernlike microstructures.

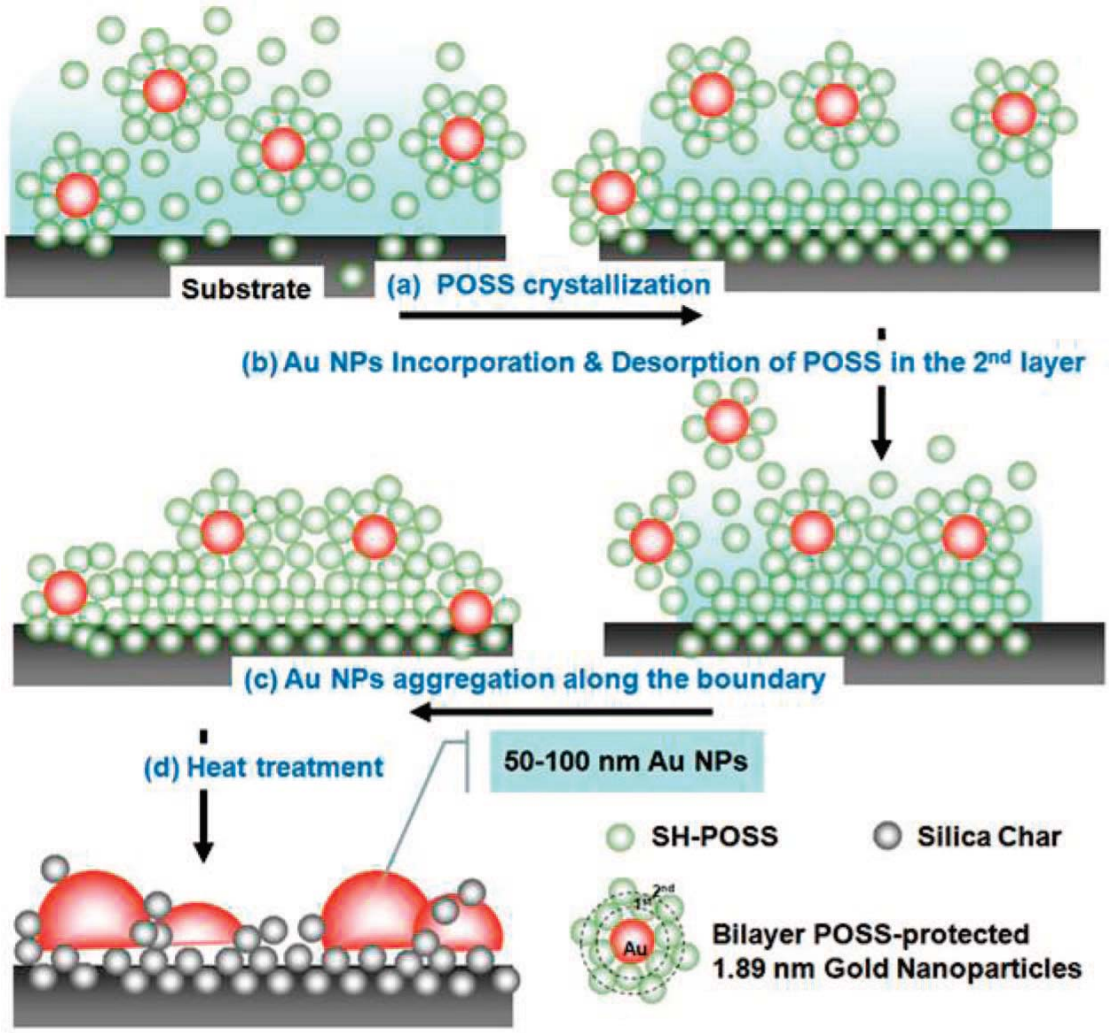

Figure 1-13. Schematic representation of the formation of fernlike POSS-Au1 microstructures.

1.3 Theory of Photoluminescence (PL)

After receiving the energy, electrons of chemical molecules excite from ground state to excited state. These molecules with high energy are unstable and transient, the energy must be released and the molecules would return to the ground state. In the process of energy release, there's many ways to choose: (1) Internal Conversion: $S_1 \rightarrow S_0$, (2) Intersystem Crossing: $S_1 \rightarrow T_1$, (3) Fluorescence: $S_1 \rightarrow S_0 + h\nu$, (4) Photochemical Reaction. Except transferred to light and released in some ways of energy release, the energy can be released by the form of heat. Only high-efficiency fluorescent (Phosphorescent) materials have more energy of excited state to release the energy.

As shown in **Figure 1-14**, a molecule may be promoted to any several vibrational levels during the electronic excitation process. In solution, however, the excess vibrational energy is immediately lost as a consequence of collisions between the molecules of the excited species and those of the solvents; the result is an energy transfer and a minuscule increase in temperature of the solvent. This relaxation process is so efficient that the average lifetime of a vibrationally excited molecule is 10^{-12} s or less, a period significantly shorter than the average lifetime of an electronically excited state. As a consequence, fluorescence from solution, when it occurs, always involves a transition from the lowest vibrational level of an excited electronic state. Several closely spaced peaks are produced, however, since the electron can return to any one of the vibrational levels of the ground state, whereupon it will rapidly fall to the lowest vibrational level of the ground electronic state by further vibrational relaxation (**Figure 1-15**). [67]

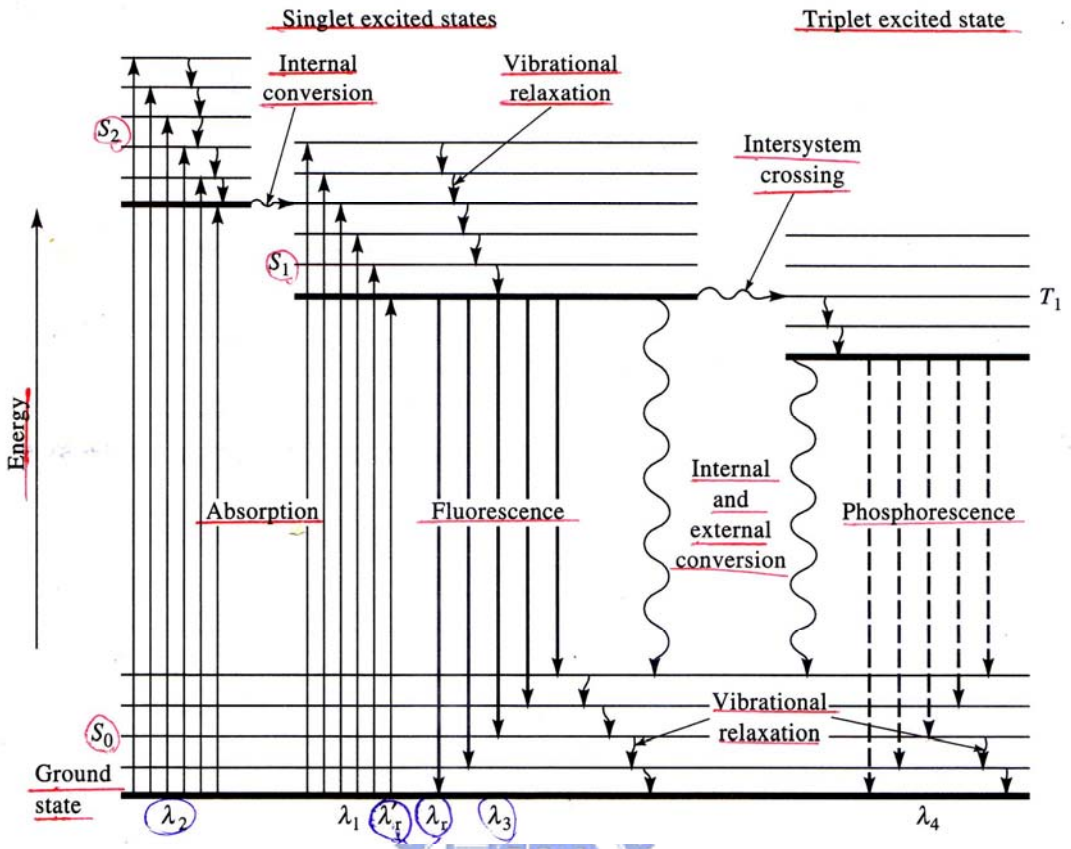

Figure 1-14. Energy diagram for a photoluminescence system.

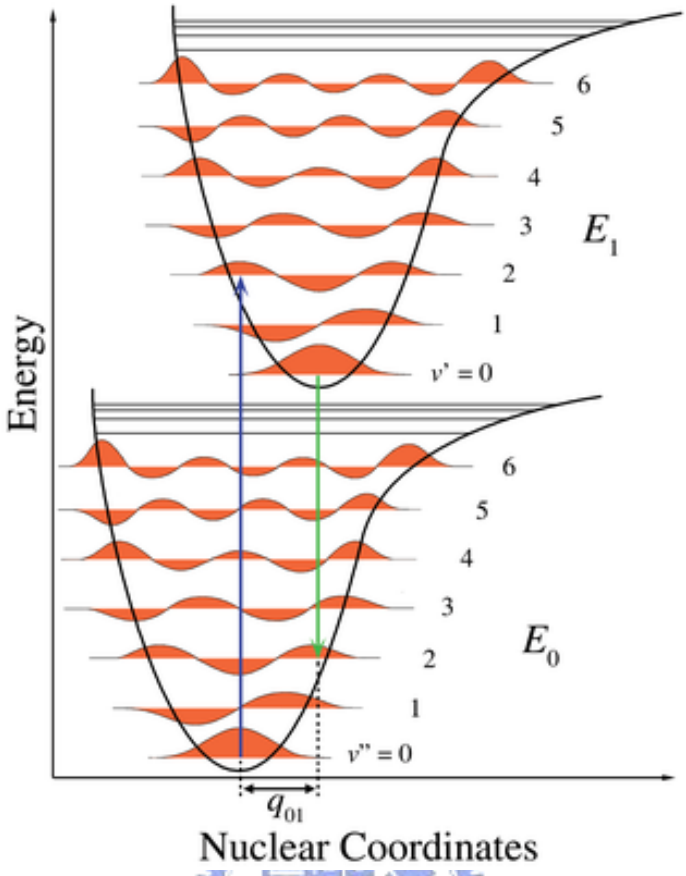

Figure 1-15. Franck-Condon principle energy diagram. Since electronic transitions are very fast compared with nuclear motions, vibrational levels are favored when they correspond to a minimal change in the nuclear coordinates. The potential wells are shown favoring transitions between $v = 0$ and $v = 2$.

1.3.1 Pyrene

Pyrene(**Figure 1-16**) is a polycyclic aromatic hydrocarbon (PAH) consisting of four fused benzene rings, resulting in a flat aromatic system. Pyrenyl photoluminescence compounds have been widely used as photosensitive probes in detecting chemical analytes such as explosively nitroaromatic compounds, oxygen, and bimolecules because pyrene has a high quantum yield (0.65 in ethanol at 293 K), long-lived excited state and a strong affinity with these analytes such as nitroaromatic compounds.[58-62] **Figure 1-17** shows the UV-Vis absorption and PL emission spectra of

pyrene.[63] The UV-Vis absorption of pyrene molecules is around 335 nm, and the fluorescence emission is around 370-450 nm. If two pyrenyl groups are close to each other (i.e. within a few Å), they can form an excited state dimer (excimer) upon excitation. Compared to excited monomers, excimers produce a red-shifted spectrum.[64-65] An excimer, as defined by Birks, is a dimer which is associated in an electronic excited state and which is dissociative in its ground state.[66] The formation of a pyrene excimer requires encounter of an electronically excited pyrene with a second pyrene in its ground electronic state. According to this definition the two pyrenes must be sufficiently far apart when light is absorbed, so that the excitation is localized on one of them. This excited pyrene, often referred to as "locally-excited" pyrene, gives rise to "monomer" emission. The observation of excimer emission indicates that diffusive encounter between the pyrenes has occurred. There are also instances where an excimer-like emission is observed, but there is no evidence that the pyrenes are separated when the light is absorbed. Because this emission strongly resembles pyrene excimer emission, many people refer to these excited species as "static excimers" (**Figure 1-18b**). By contrast, excimers which satisfy the Birks definition are referred to as "dynamic excimers" (**Figure 1-18a**).[67]

Figure 1-16. Chemical structure of pyrene.

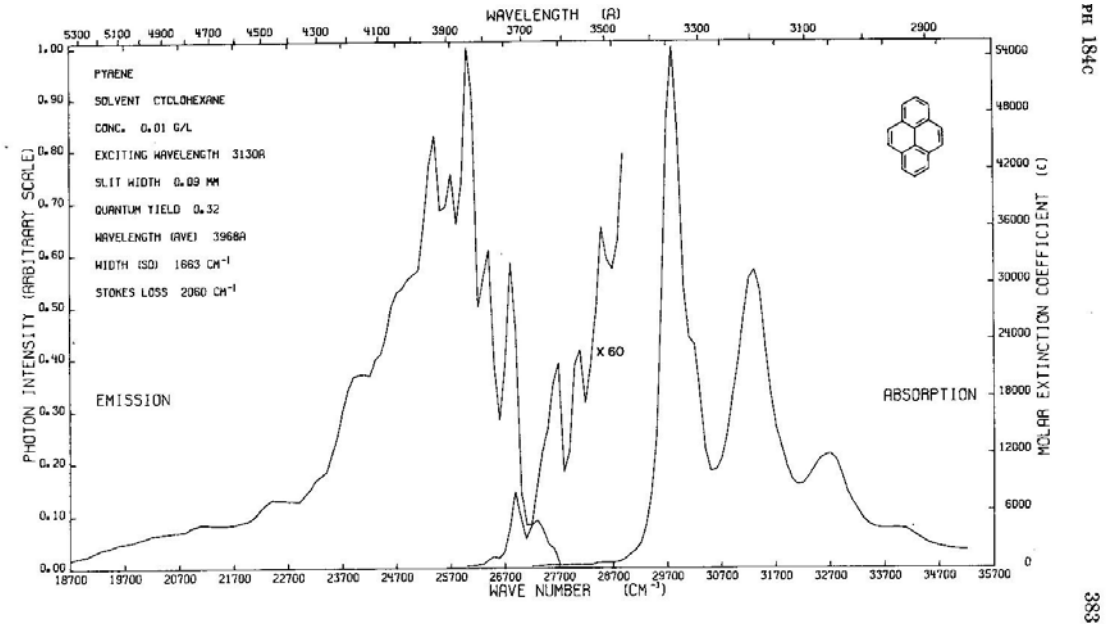

Figure 1-17. UV-Vis and PL spectra of pyrene.

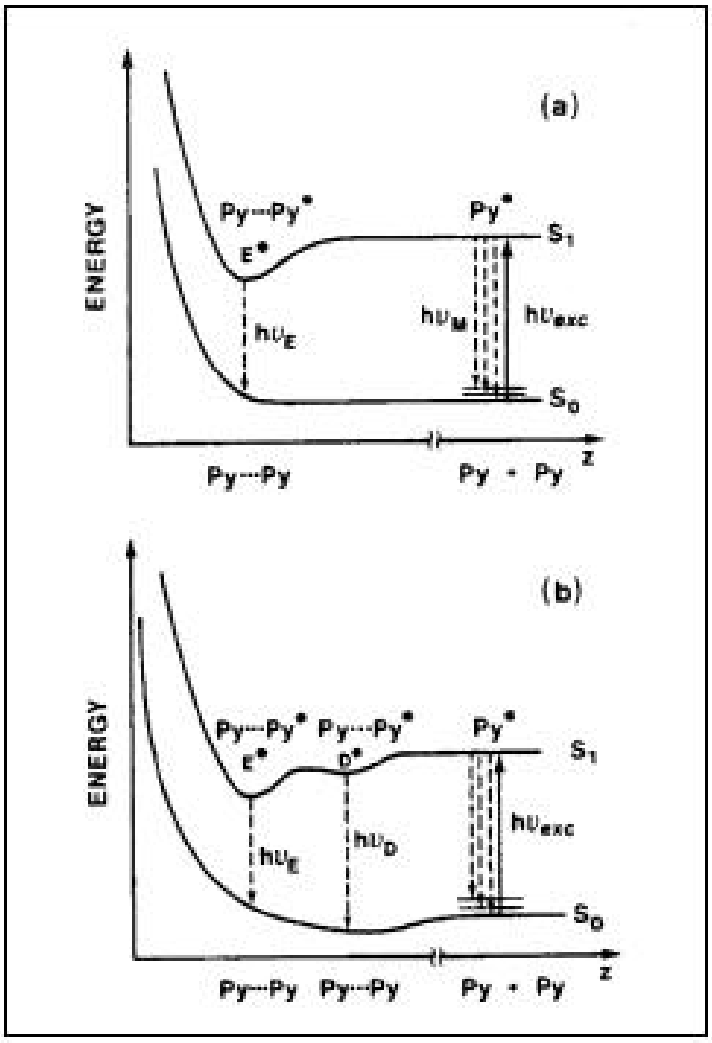

Figure 1-18. Schematic potential energy diagrams for pyrene excimer formation.

1.3.2 Fluorescent Chemosensor

Fluorescent chemosensors capable of selectively recognizing cations have potential analytical applications in many different fields, including chemistry, biology, and medicine.[68-71] Most of the fluorescent chemosensors for cations are composed of a cation recognition unit (ionophore) together with a fluorogenic unit (fluorophore) and are called fluoroionophores.[70] An effective fluorescence chemosensor must convert the event of cation recognition by the ionophore into an easily monitored and highly sensitive light signal from the fluorophore.[72] As fluorogenic units, pyrenes (Py) are one of the most useful because of their relatively efficient excimer formation and emission.[73] In Kim's[74] paper, A 1,3-alternate calix[4]crown platform provides a crown ether ring for metal ion complexation to detect the Pb^{2+} and K^{+} ions. The mechanism of binding with Pb^{2+} was shown in **Figure 1-19**. Binding with Pb^{2+} was result in weak excimer emission, however, when adding K^{+} ion, alkali metal cations are bound by the crown-5 ring and hardly affects the excimer stability, and little change in its emission intensity is observed (**Figure 1-20)**.

In Hideya Yuasa's[75] work, the ring flip of a carbohydrate is employed for the tongs-like movable component of a metal ion sensor. A pair of separated pyrene groups attached to the carbohydrate component is placed side by side when it recognizes metal ions, affording excimer fluorescence. This molecular sensor is selective for Zn^{2+} and Cd^{2+}; the mechanism is shown in **Scheme 1-5**.

For anions, Kim's groups also do the research work on the detection of F^{-}.[80] Calixarene-based fluorescent chemosensor with two fluorogenic pyrene units conjugated to amide groups as guest recognition sites is synthesized. Complexation of F^{-} causes a red shift of its absorption band to 400 nm ($\Delta\lambda$=54 nm) and a blue shift of the excimer emission to 470 nm ($\Delta\lambda$=12 nm) together with enhanced fluorescence

intensity. The blue-shifted excimer emission is attributed to a pyrene dimer formed in the ground state, a so-called static excimer (**Figure 1-21**).

Besides detection of cations[74-79], anions[80-81] and biomolecules[82-85], detection of nitroaromatic compounds (NACs) [59, 81] would be important. An ester (PBPOSS) of 1-pyrenebutyric acid (PBA) and POSS was synthesized by Hua Bai and co-workers.[81] Upon exposure to the vapours of nitroaromatic compounds, including trinitrotoluene and dinitrotoluene, the films show fast fluorescence quenching. The high performance of these gas sensors is due to the high excimer contents and good vapour permeability of the PBPOSS films (**Figure 1-22**).

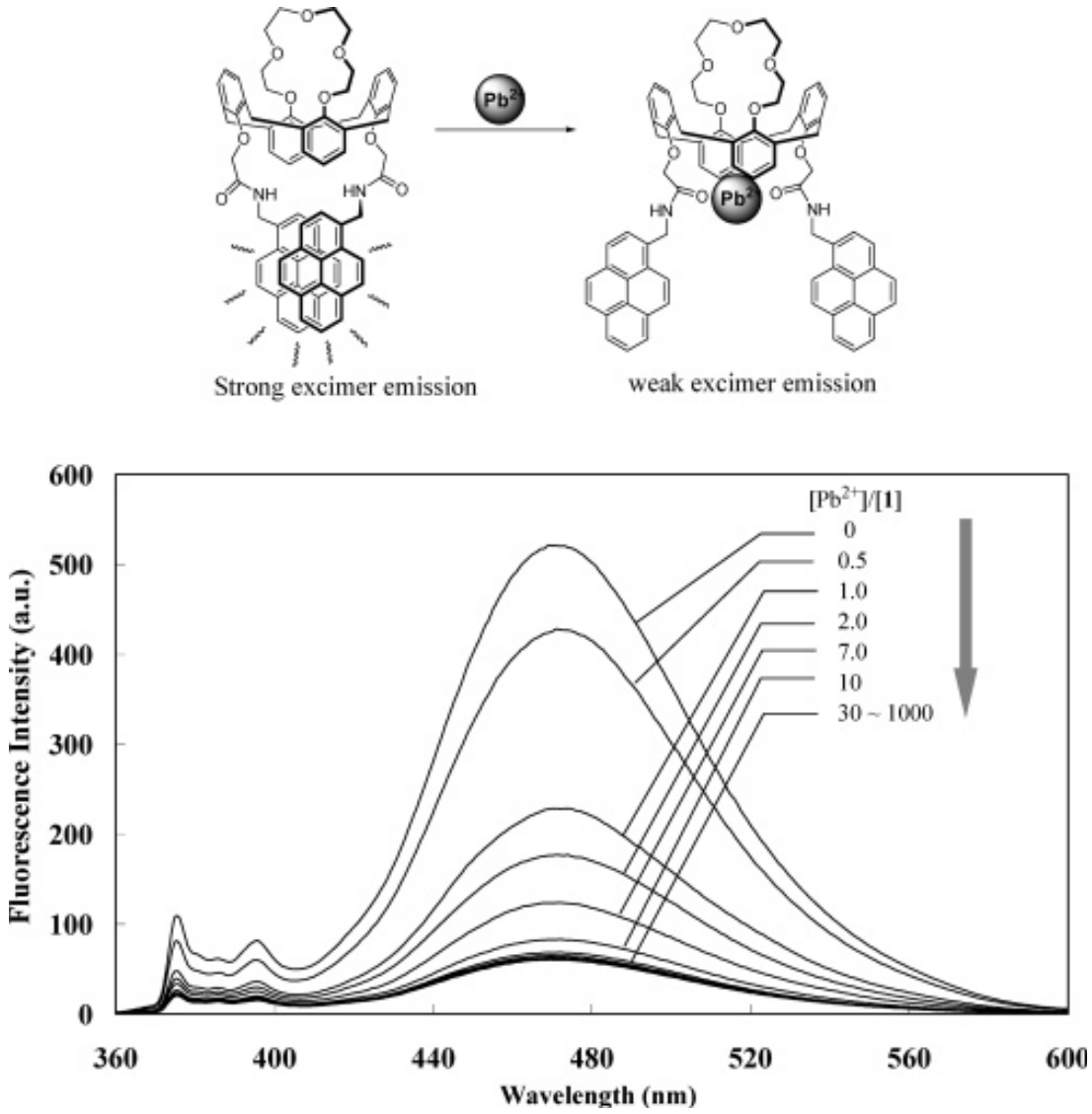

Figure 1-19. Effect of added Pb^{2+} on the fluorescence emission spectra in MeCN.

(The excitation wavelength was 344 nm.)

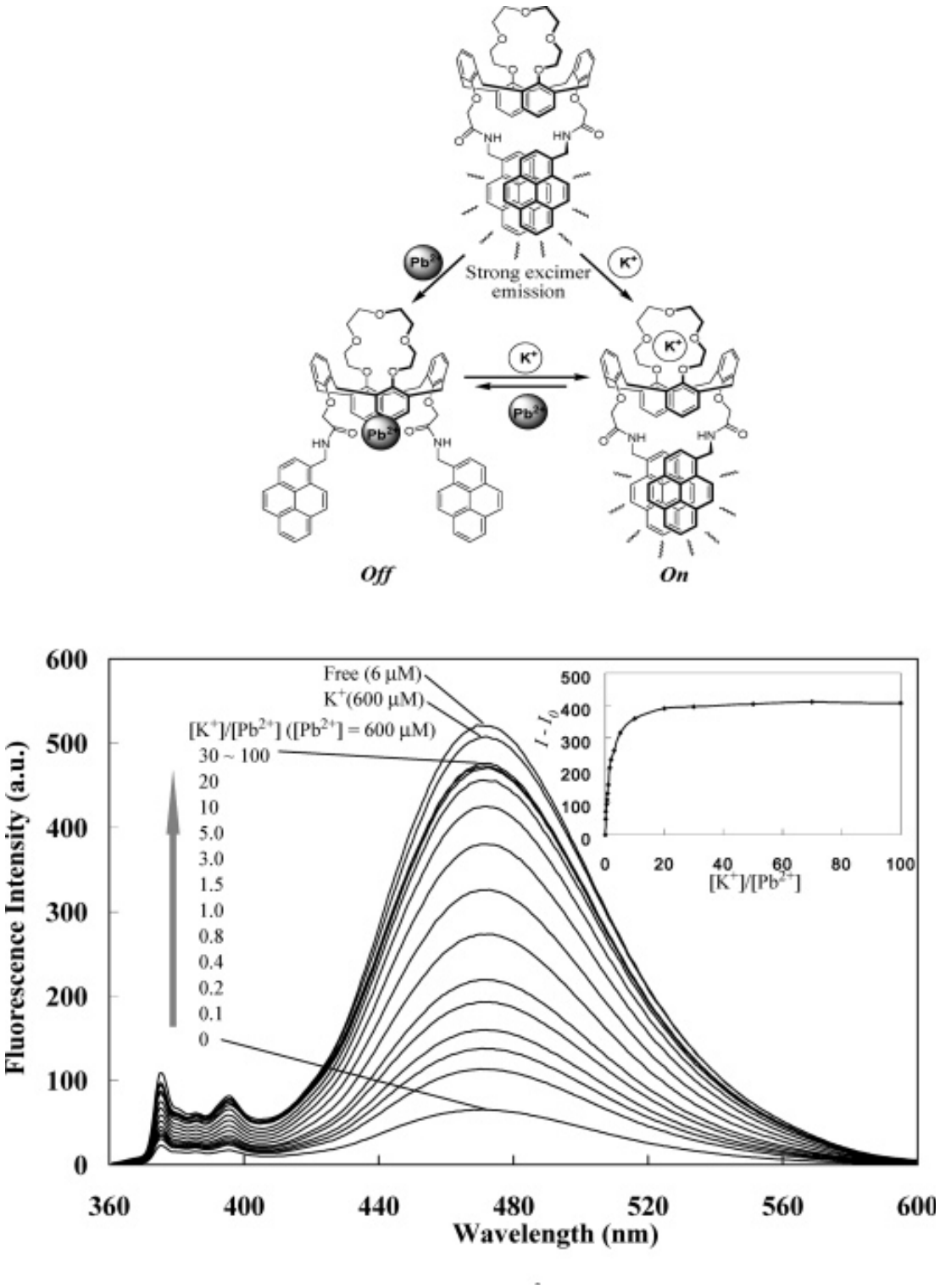

Figure 1-20. Fluorescence emission changes for the Pb^{2+} complex in MeCN upon addition of K^+. (The excitation wavelength was 344 nm.)

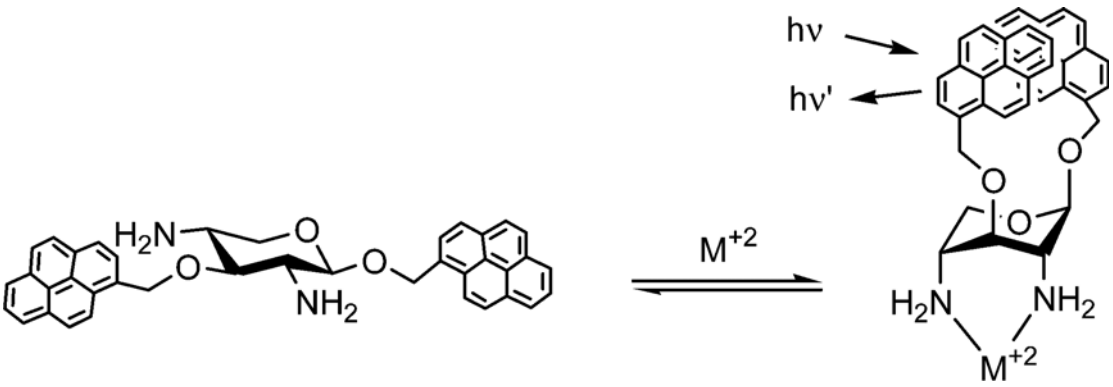

Scheme 1-5. Mechanism of binding with M^{2+}.

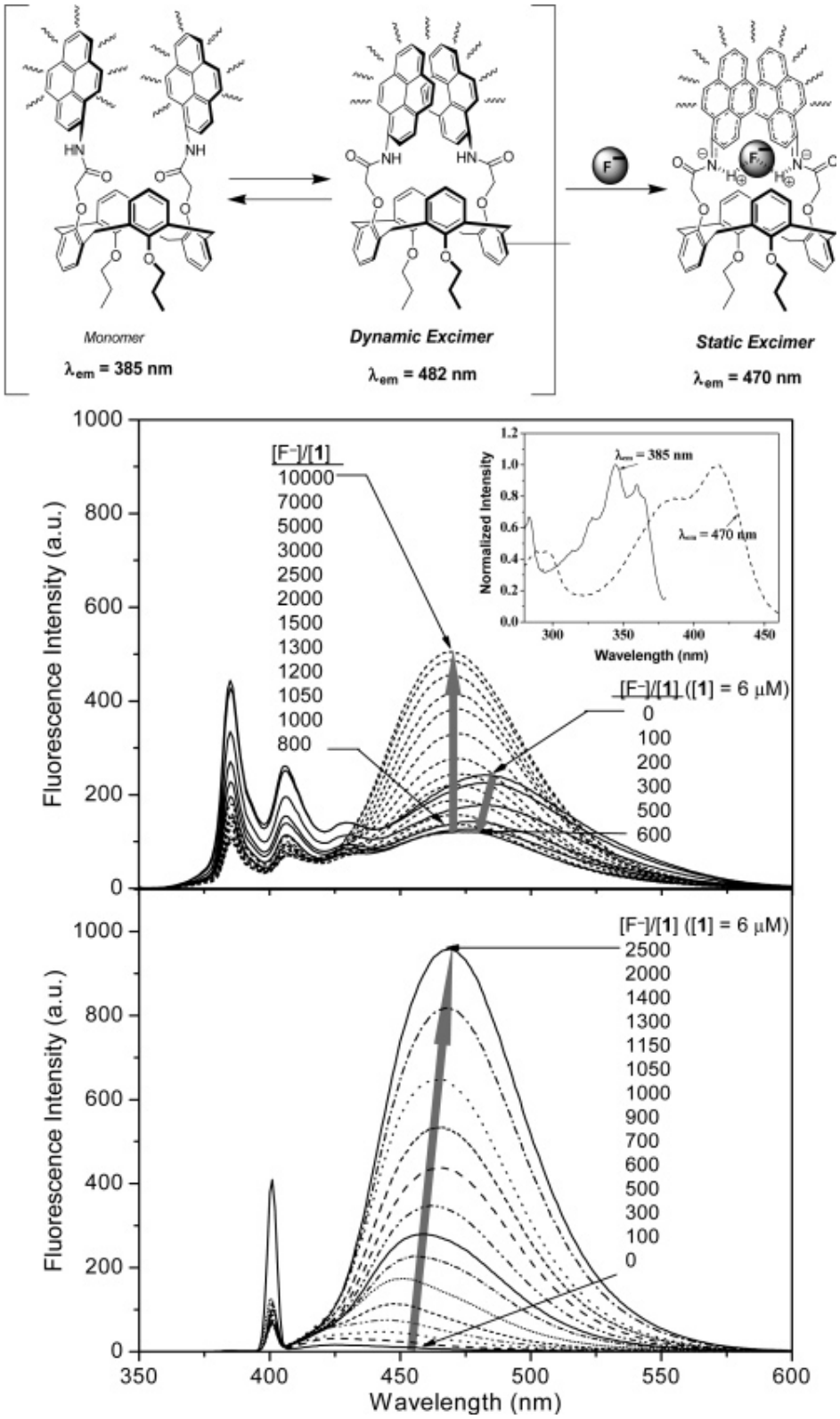

Figure 1-21. Fluorescence spectra of **1** (6.0 μM) upon titration with $Bu_4N^+F^-$ in MeCN. Excitation wavelengths were (a) 346 and (b) 400 nm, respectively. Inset: excitation spectra (normalized) monitored at 385 (solid line) and 470 nm (dashed line) in the presence of 1000 equiv of $Bu_4N^+F^-$.

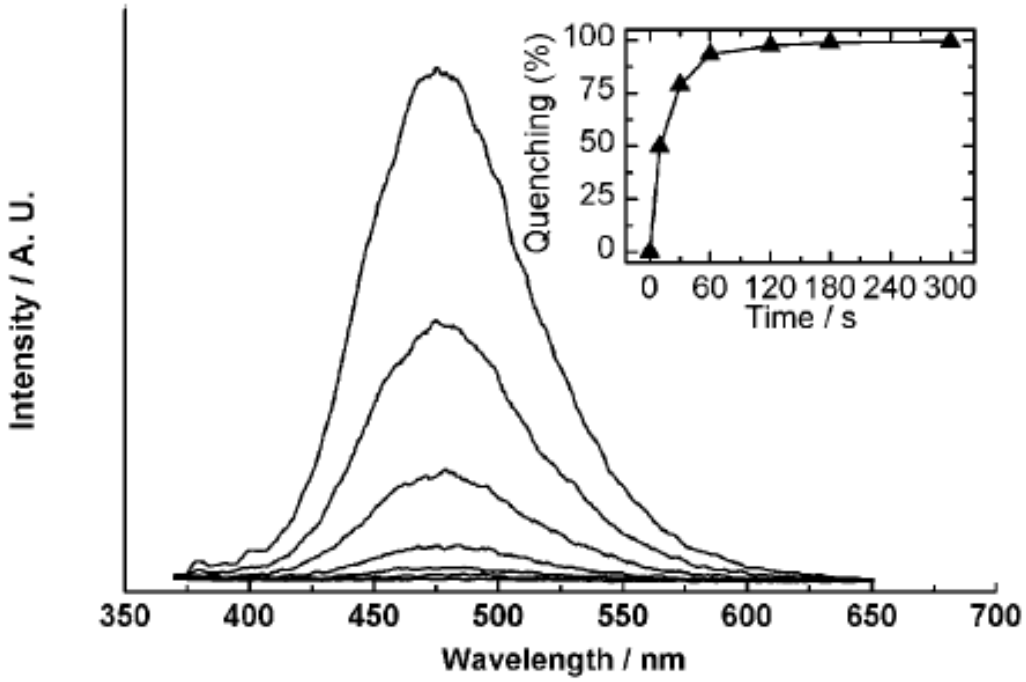

Figure 1-22. Fluorescence spectra of a 9 nm thick PBPOSS film upon exposure to TNT vapor for different times. From top to bottom, the exposure time was 0, 10, 30, 60, 120, 180 and 300 s, respectively. Inset: plot of quenching efficiency (%) versus time.

Chapter 2

Motivation

POSS molecules can be regarded as core-shell colloids with solvated alkyl or aryl shells to disperse insoluble siloxane cores in solvents.[11-24] Thus, the solvent effect plays an important role in the crystallization of POSS colloids. As reported, the X-ray diffraction patterns (XRD) revealed that the dimension ratios (*c*/*a*) of hexagonal unit cells for POSS crystals measured around 1.06, quite smaller than the theoretical ratio of 1.63 for a hexagonal closed packing model of hard spheres. These results of XRD studies indicated the extension of the lattice constant *a* between two adjacent POSS colloids on the basal plane of a unit cell and the compression of the lattice constant *c* between those in the c-axis direction of a unit cell. Our previous study suggested that such platelike hexagonal unit cells with the dimension ratios (*c*/*a*) of 1.06 can be arranged in a defined and a periodic manner to form crystalline POSS thin films.[15-18] As a result, on the surface of a POSS crystal, the ordered pattern of "small holes" with the regular distance of the lattice constant *a* to one another is able to function as a template, similar to a egg rack, to disperse and allocate POSS derivatives such as POSS-protected Au nanoparticles.[15] Consequently, it is a unique characteristic that POSS crystals can be used a template to self-assemble other functional molecules or nanoparticles on its surface through POSS-POSS recognition.

Pyrenyl chromophores have been widely used as photosensitive probes in detecting chemical analytes such as nitroaromatic compounds, oxygen, and biomolecules because the high-quantum-yield emissions of pyrenyl excimers, a short-lived dimer with the π-π stacking of two adjacent pyrenyl rings can be quickly quenched with these analytes through energy transfers.[58-62] Many literatures reported on photoluminescence (PL) sensors using pyrenyl excimers in solution, but there are not a lot of studies using them in the thin films.[80,86-87] The latter gives people a quicker

response than the former to detect toxic or explosive gases such as nitrobenzene and trinitrotoluene when these gases are exposed to the circumstances. However, it is still a challenge to develop a method of spreading these pyrenyl chromophores on a given substrate. As is well known, spin-coating is one of the most convenient techniques to fabricate such a photoluminescent thin-film. Unfortunately, the spin-coating pyrenyl film shows only a weak excimer emission due to a random packing of pyrene rings at a rapid rate of solvent evaporation in addition to large loss of sample solutions.[61,88] Therefore, Fujiwara et al[60,88] synthesized a carboxylic acid-functional pyrenyl derivative, associated with another through the intermolecular hydrogen bond to form the dimer-like structure with strong visible emission for application of sensing oxygen. However, these network structures composed with physically intermolecular hydrogen bonds can retarded the diffusion of the analytes with large molecular sizes such as trinitrotoluene, TNT, resulting in the relatively low response rate of the excimer quenching for these compounds. Consequently, the perfect microstructure for these PL sensors is to disperse these pyrenyl chromophores on a given substrate or template as thin as possible.

Recently, many literatures reported that the aggregations through π-π stacking of conjugated PL units could be effectively inhibited by physically blending or chemically grafting with bulky POSS nanoparticles in the application of the high-performance active layers of organic molecular and polymeric light-emitting diode devices (OLED[89-95] and PLED[96-103]). As reported,[81] pyrene-monofunctional isobutyl-POSS (Py-POSS) was successfully synthesized by Bai et al and its spin-coating films showed the rapid fluorescent response to the detection of explosive TNT vapor. Unfortunately, they didn't study the effect of the unique POSS crystal structure on the PL sensors. Herein, bispyrenyl-monofunctional isobutyl-POSS (BPy-POSS) was synthesized and characterized. As the chemical structure shown in

Figure 2-1a, we expect that BPy-POSS has a thermodynamically driven tendency to form an intramolecular excimer, the close form of butterfly-like microstructure, through the free rotation of two ether bonds. So, excimer conformation is more easily produced by intramolecular ether bonds than that by intermolecular hydrogen bonds between two carboxylic acid-functional pyrenes. In addition, we blended BPy-POSS and inert isobutyl-POSS (i-Bu POSS) to give the template composed of crystal i-Bu POSS thin films and to disperse BPy-POSS on its surface small holes (**Figure 2-1b**).

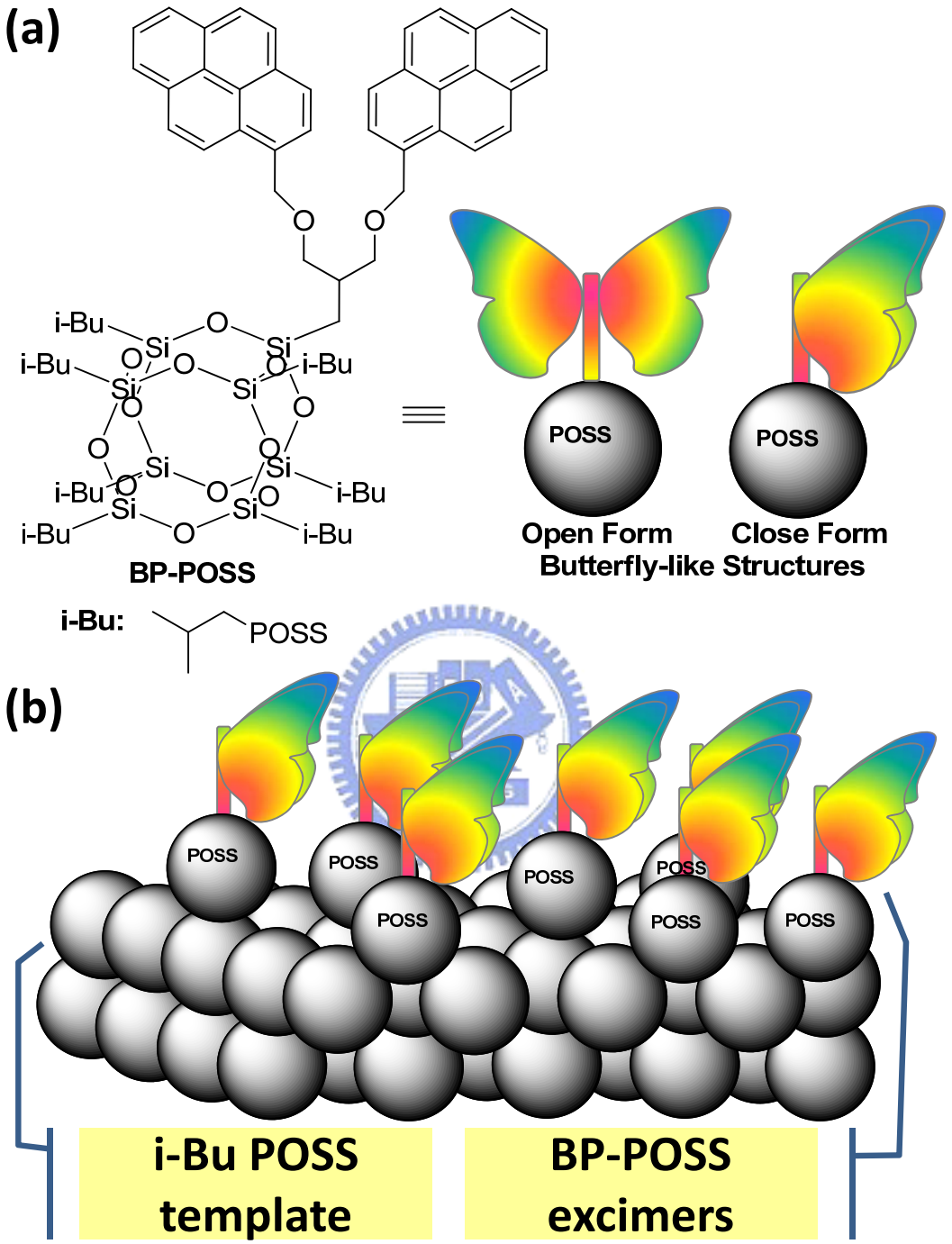

Figure 2-1. (a) Open and close forms of BPy-POSS microstructure, (b) thin film of blend of BPy-POSS and i-Bu POSS.

Chapter 3

Experimental Section

3.1 Materials

1. 1-pyrenemethanol

Aldrich, 98%

MW: 232.28 g/mol

CAS: 24463-15-8

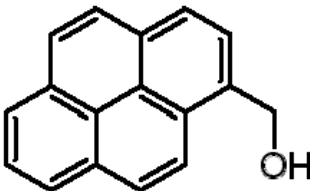

2. 3-Chloro-2-chloromethyl-1-propene (methallyl dichloride)

ACROS, 99%

MW: 125 g/mol, d=1.08 g/ml

CAS: 1871-57-4

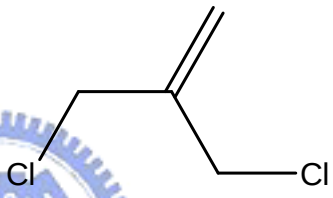

3. Potassium hydride

ACROS, 25－35 wt. %, dispersion in mineral oil

MW: 40.11 g/mol

CAS: 7693-26-7

4. Trichlorosilane

Aldrich, 99%

MW: 135.45 g/mol, d=1.342 g/ml

CAS: 10025-78-2

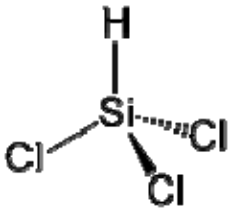

5. Trisilanolisobutyl POSS®

Hybrid Plastics

MW: 791.41 g/mol

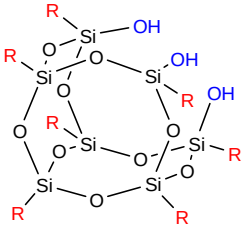

6. Triethylamine

TEDIA, >99%

MW: 101.19 g/mol, d＝0.726 g/ml

CAS: 121-44-8

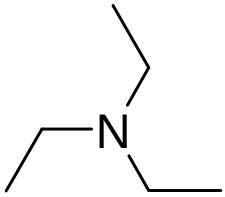

7. Platinum(0)-1, 3-divinyl-1,1,3,3-tetramethyldisiloxane complex solution

[Pt(dvs)] in xylene (Pt ~2%)

Aldrich

MW: 381.48 g/mol, d=0.855 g/ml

CAS: 68478-92-2

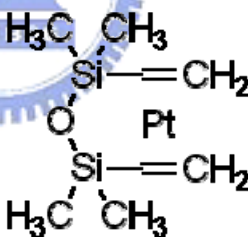

8. Octa isobutyl-POSS (i-Bu POSS)

Hybrid Plastics

MW: 873.59 g/mol

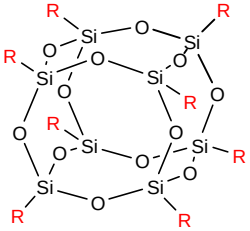

9. Tetrahydrofuran

TEDIA, 99.8%

MW: 72.11 g/mol, d = 0.886 g/ml,

boiling point: 65~67 °C

CAS: 109-99-9

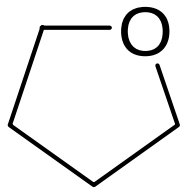

10. Toluene

TEDIA, 99.5%

MW: 92.14 g/mol, d=0.865 g/ml

CAS: 203-625-9

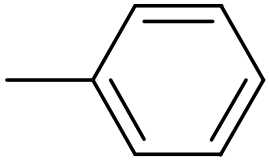

11. Calcium Hydride

ACROS, 99%

MW: 42.09 g/mol

CAS: 7789-78-8

3.2 Purification of Solvents

3.2.1 THF

Potassium hydride dispersion in mineral oil (30%) was put in a dry round bottomed flask under Argon atmosphere; hexane was added and stirred for 10 minutes to dissolve the mineral oil. After stated for a while, the liquid was sucked by syringe and thrown away. Repeat this process three times, the residual were dried by the vacuum pump to ensure that there's no mineral oil and hexane remained. THF was added via syringe and stirred for 12 hours under Argon atmosphere. After completely mixed, THF was distilled at 80 °C.

3.2.2 Toluene

Toluene, calcium hydride and a magnetic stirrer were placed in a dry round bottomed flask under Argon atmosphere; after stirred for 12 hours, toluene was distilled at 110 °C.

3.3 Synthesis of Hydride-monofunctional Isobutyl-POSS (Si-H iBu-POSS)

Hydride-monofunctional isobutyl-POSS (Si-H iBu-POSS) was synthesized by sol-gel reaction between trisilanolisobutyl POSS® and trichlorosilane ($HSiCl_3$) in anhydrous THF using triethylamine (TEA) to capture HCl in form of an ammonium salt (**Scheme 2-1a**). Under Argon atmosphere, Si-H iBu-POSS was obtained by adding a slight excess of $HSiCl_3$ (1.21 ml, 12 mmol) to a 1-liter flask containing TriSilanolIsobutyl POSS® (7.91 g, 10 mmol), TEA (5.01 ml, 36 mmol) and 800ml anhydrous THF. The reaction flask was stirred under Argon for 12 hours, followed by filtration to remove the $HNEt_3Cl$ salts. Si-H iBu-POSS was purified by precipitation from excess ethanol. The 87% yield of Si-H iBu-POSS (11.6 g, 8.7 mmol) was isolated after vacuum drying. Proton nuclear magnetic resonance (^1H NMR) (δ, $CDCl_3$): 0.61 (m, 14H, $SiCH_2$), 0.97 (m, 42H, CH_3), 4.11 (s, 1H, SiH).

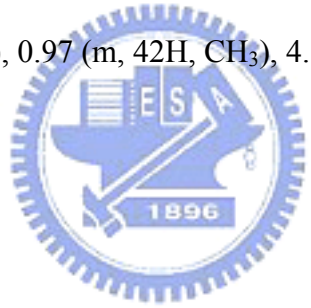

3.4 Synthesis of Vinyl-functional Bispyrene (V-BPy)

The vinyl-functional bispyrene (V-BPy) was prepared by etherification reaction of an excess of 1-pyrenemethanol (Py-OH) with methallyl dichloride in anhydrous THF using a strong base of potassium hydride (KH) (**Scheme 2-1b**). Dry KH (0.43 g, 10mmol, purification by washing with hexane), Py-OH (2.2 g, 9.5 mmol) and freshly distilled THF (30 ml) were placed in a dry round bottomed flask under Argon atmosphere. At room temperature, methallyl dichloride (0.37 ml, 3.2 mmol) was added to the flask with mixture drop by drop. The mixture was stirred at room temperature for 15 min and stirred at 65 °C for 12 hours. After cooling to room temperature, the reaction mixture was quenched by water and extracted with dichloromethane. The organic layer then dried over anhydrous $MgSO_4$ and the solvent was removed under vacuum. Purification of the residue by flash column chromatography on silica gel with the same amount of hexane and dichloromethane and yielded 1.32 g of the V-BPy solid (80% yield). ^{1}H NMR (δ, $CDCl_3$): 4.21 (s, 4H, $CC\underline{H_2}O$), 5.18 (s, 4H, $OC\underline{H_2}$), 5.34 (s, 2H, $C\underline{H_2}CCH_2O$), 7.9-8.3 (m, 18H, aromatic).

3.5 Synthesis of Bispyrene-monofunctional isobutyl-POSS (BPy-POSS)

The bispyrene-monofunctional isobutyl-POSS (BPy-POSS) was prepared by hydrosilylation reaction of an excess of vinyl-functional bispyrene (V-BPy) with hydride-monofunctional isobutyl-POSS (Si-H iBu-POSS) in anhydrous toluene at 60 °C using a platinum(0) catalyst [Pt(dvs)] (**Scheme 2-1b**).[9,104-105] A solution of Si-H iBu-POSS (2.5 g, 3 mmol) and V-BPy (15.5g, 30mmol) in toluene (60 mL) in a 100-mL Schlenk flask equipped with a reflux condenser and a magnetic stirrer was heated at 60 °C under argon and then Pt(dvs) (0.2 ml, 0.4 μmol) was added via syringe. The reaction, which was monitored by measuring the decrease in intensity of the FT-IR spectra signal at 2134 cm^{-1} for the Si-H bonds, was complete after 24 hours. The yellowish, transparent reaction mixture became clear after removal of the Pt(dvs) catalyst through flash chromatography (neutral Al_2O_3; toluene). The crude product was purified by flash column chromatography on silica gel with hexanes-ethyl acetate (EA: Hexane=1: 8) to yield BPy-POSS (2.5 g, 62%). ^{1}H NMR (δ, $CDCl_3$): 0.61 (s, 16H, $SiC\underline{H}_2$), 0.95 (s, 42H, $C\underline{H}_3$), 1.86 (m, 8H, $SiCH_2C\underline{H}$), 3.66 (m, 4H, $CHC\underline{H}_2O$), 5.06 (s, 4H, OCH_2), 7.8-8.21 (m, 18H, aromatic).

3.6 Preparation of i-Bu POSS and BPy-POSS blends

BPy-POSS (0.5 mg) and i-Bu POSS (9.5 mg) were dissolved in 1 ml solvent to fabricate the 5 wt% BPy-POSS/ i-Bu POSS blend solution; BPy-POSS (2 mg) and i-Bu POSS (8 mg) were dissolved in 1ml solvent to make the 20 wt% BPy-POSS/ i-Bu POSS blend solution. The blend solutions were stirred for 2 hours then the solvent was removed by rotary evaporator. To avoid the residual solvent remained, the samples were put into the vacuum oven for 1 day.

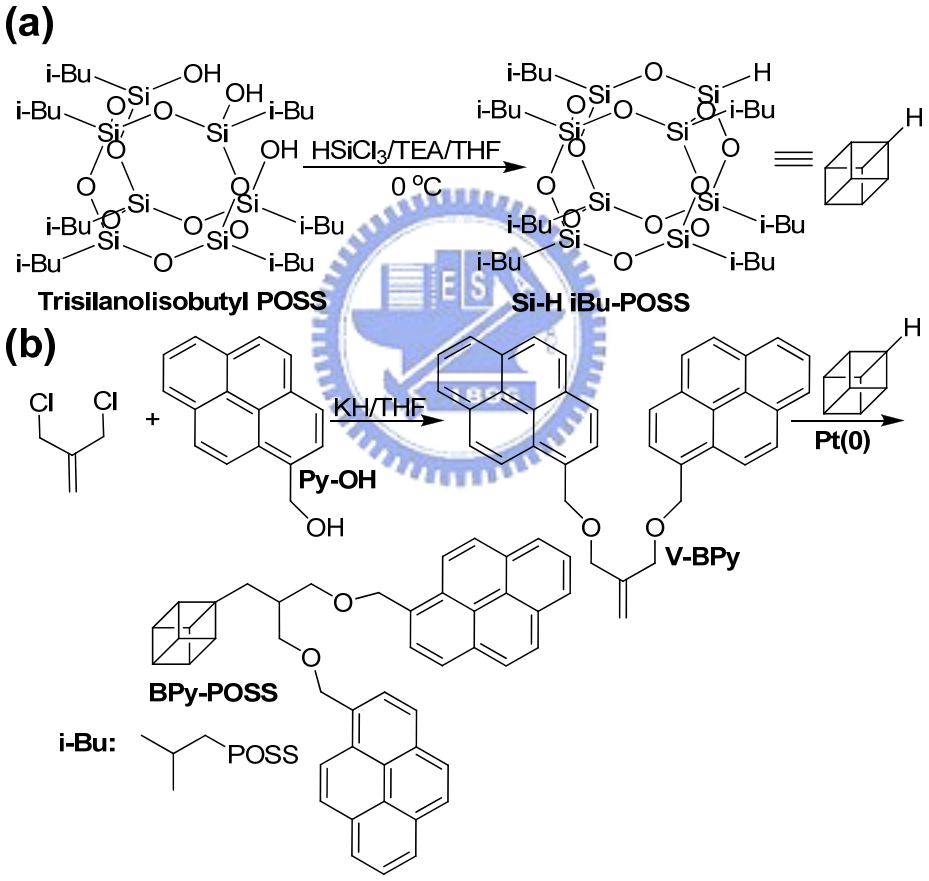

Scheme 3-1. Synthesis of (a) Si-H iBu-POSS and (b) BPy-POSS.

3.7 Characterization

3.7.1 NMR Spectroscopy

^{1}H NMR solution spectra were obtained using Varian Unity 300Hz instrument; *d*-chloroform was the solvent. High-resolution solid-state ^{29}Si NMR spectroscopy experiments were performed at 25 °C using a Bruker DSX-400 spectrometer operating at a resonance frequency of 79.375 MHz. High-resolution solid state ^{29}Si NMR spectra were acquired with a 90 °C pulse width of 5 μs, a pulse delay time of 2 s, and with the spin rate of 6500Hz. The total range of ^{29}Si is from 231.99 ppm to -292.939 ppm.

3.7.2 Matrix-Assisted Laser Desorption Inoization-Time of Flight Mass Spectrometry (MALDI-TOF MS)

A Mass spectrum was obtained using a Bruker Daltonics Autoflex Ⅲ TOF-TOF mass spectrometer. The following voltage parameters were employed: ion source 1, 19.06 kV; ion source 2, 16.61 kV; lens, 8.78 kV; reflector 1, 21.08 kV; reflector 2, 9.73 kV. The laser power was set to 45 % with a frequency of 10 Hz, while the mass spectrum was collect from 300 shots. The α-cyano-4-hydroxycinnamic acid (CHCA) was premixed in 33.3% acetonitrile solution to make the matrix solution. The BPy-POSS was mixed with matrix solution at the ratio 1:1. The $AgNO_3$ was added for the purpose of ionization of BPy-POSS to become BPy-POSS/ Ag^{+} complex. Then the sample was submitted to analysis with MALDI-TOF.

3.7.3 Differential Scanning Calorimetry (DSC)

Thermal analysis was performed with a differential scanning calorimeter from DuPont (DSC-Q20) with a heating rate of 10 °C/min, a cooling rate of 5 °C /min and a temperature range of -90-200 °C. Temperature and energy calibrations were carried

out with indium. The measurements were made with a 5-10 mg sample in a DSC sample cell; in first scan, the sample was heated from room temperature to 200 °C, after the first heating run, the samples were then cooled to -90 °C and heat again to 200 °C to examine the temperature of glass transition (T_g) and the other transition temperatures.

3.7.4 Thermal Gravimetric Analysis (TGA)

Thermal Gravimetric Analysis (TGA) is a simple analytical technique that measures the weight loss (or weight gain) of a material as a function of temperature. The weight loss over specific temperature range indicate the decomposition of the sample, thermal stability and absorbed moisture content, etc. After the sample treatment, various concentration of BPy-POSS/ i-Bu POSS samples were recorded using a TGA-Q50 (TA, USA) over a temperature range of 50-750 °C in a inert atmosphere, at a heating rate of 10 °C/min.

3.7.5 Ultraviolet-Visible spectroscopy (UV-Vis)

UV-Vis absorption spectroscopy is the measurement of the attenuation of a beam light after it passes through a sample or after it reflects from a sample surface. Both the shape of the peak(s) and the wavelength of maximum absorbance (λ_{max}) give information about the structure of the compound. The sample solutions were put in the quartz holder and the sample films should be coated on quartz glass. In our experiment, UV-Vis spectra were measured using an HP 8453 diode-array spectrophotometer.

3.7.6 Photoluminescence Spectroscopy (PL)

PL spectrophotometer was used to measure the photoluminescence wavelength of

sample film or solution. PL spectra were obtained using a Hitachi F-4500 luminescence spectrometer. The sample solutions were put in the quartz holder and the sample films should be coated on quartz glass. Then the spectrophotometer emitted a source light to excite the sample; the wavelength of the source light was determined by the UV absorption of samples. We used toluene and dichloromethane as the solvent.

3.7.7 X-Ray Powder Diffraction (XRD)

X-ray powder diffraction (XRD) is a rapid analytical technique used for phase identification of a crystalline material and can provide information on unit cell dimensions. The techniques are based on observing the scattered intensity of an X-ray beam hitting a sample as a function of incident and scattered angle. The sample solutions we had prepared in toluene were dropped on a cleaned wafer surface, after solvent evaporating, we put the wafer into the XRD sample holder. The XRD patterns were collected using a D8 Advance Powder X-ray diffractometer (Cu Kα, 40 kV/ 40 mA; Bruker, Germany). The scanning rate was 0.6 °/min from 2θ =5 ° to 30 °. Data were collected and plotted as intensity versus 2θ.

3.7.8 Confocal Microscopy

Confocal microscopy is an optical imaging technique used to increase micrograph contrast and/or to reconstruct three-dimensional images by using a spatial pinhole to eliminate out-of-focus light or flare in specimens that are thicker than the focal plane. The entire specimen is flooded in light from a light source. Due to the conservation of light intensity transportation, all parts of the specimen throughout the optical path will be excited and the fluorescence detected by a photodetector or a camera. We used the

Leica TCS SP5 Confocal Spectral Microscope Imaging System in NTU, the excited light source is 100 mW Ar blue lasers; the fluorescence microscopy is Leica DMI 6000B CS.

One drop of dilute toluene solutions (10 mg/ml of BPy-POSS/ i-Bu POSS blends solution) was placed onto a glass, and then air-dried at 25 °C.

3.7.9 Atomic Force Microscopy (AFM)

The Atomic Force Microscopy (AFM) is a very high-resolution type of scanning probe microscope, with demonstrated resolution of fractions of a nanometer, The AFM consists of a microscale cantilever with a sharp tip (probe) at its end that is used to scan the specimen surface. The Atomic Force Microscopy (AFM) employed in this study is a Digital Instruments Veeco Dimension 5000 Scanning Probe Microscope (Veeco Metrology Group). The AFM tapping mode with a 5-10 nm radius silicon tip was used to scan the surface structure, the displacement resolution of AFM is about 0.1 nm. One drop of dilute toluene solutions (10 mg/ml of BPy-POSS/ i-Bu POSS blends solution) was placed onto a wafer, and then air-dried at 25 °C.

3.7.10 Transmission Electron Microscopy (TEM)

Transmission electron microscopy (TEM) is a microscopy technique that a beam of electrons is transmitted through ultrathin specimen, interacting with the specimen as it passes through. An image is formed from the interaction of the electrons transmitted through the specimen; the image is magnified and focused onto an imaging device, such as a fluorescent screen. The dark areas of the image correspond to areas on the specimen where fewer electrons were able to pass through; the lighter areas are where more electrons did pass through.

For Transmission Electron Microscopy studies, ultrathin sections of the sample

were prepared using a Leica Ulatracut UCU microtome equipped with a diamond knife. Slices of ca. 700 Å thicknesses were cut at room temperature and then the samples were transferred onto the carbon-coated Cu TEM grid. The samples weren't stained.

TEM analysis was performed using a Hitachi H-7500 electron microscope operated at 100 kV.

3.7.11 Dynamic Light Scattering (DLS)

The hydrodynamic diameter, D_h, of the BPy-POSS and i-Bu POSS solution (in toluene) was measured by dynamic light scattering (DLS).

DLS measurements were performed on Brookheaven 90 plus model equipment (Brookheaven Instruments Corporation, USA) with a He-Ne laser with a power of 35 mW at 632.8 nm. The temperature was controlled at 25 °C, and the measurements were done at an angle of 90 °. All the solutions have been filtered before DLS measurements.

Chapter 4

Results and discussion

4-1 Synthesis of BPy-POSS

The procedure of hydrolytic condensation of monofunctional trichlorosilane in aqueous acetone for synthesis of incompletely condensed trisilanol alkyl-POSS (T7-POSS) has been described by Feher et al. and Schmid et al.[107-108] An efficient method for preparing such monofunctional POSS with full condensed siloxane-oxygen frameworks involves the corner-capping of T7-POSS with a variety of trichlorosilane coupling agents. Thus, Si-H iBu-POSS was prepared by condensation of trisilanolisobutyl POSS® with trichlorosilane, providing BPy-POSS by followed hydrosilylation with V-BPy. Due to the commercial T7-POSS with a small amount of completely condensed isobutyl POSS, trisilanolisobutyl POSS® can be purified by hydrogen bonding-driven dissolving in anhydrous ethanol before condensation with trichlorosilane. In comparison with **Figures 4-1a** and **Figure 4-1b**, the hydrosilane (Si-H, peak *d*) signal at 4.11 ppm was observed in the product of Si-H iBu-POSS by ^{1}H NMR spectra. V-BPy was synthesized by etherification of methallyl dichloride and Py-OH using KH in anhydrous THF. Thus, the shift from peak *f* to *f'* and the signals of ether (peak *g* at 4.26 ppm) and vinyl groups (peak *h* at 5.35 ppm) are detected for V-BPy by ^{1}H NMR spectra (**Figures 4-1c** and **Figure 4-1d**) result from the formation of a ether linkage between methallyl dichloride and Py-OH. The desired product of BPy-POSS was obtained by the followed hydrosilylation of V-BPy with Si-H iBu-POSS. Herein, only β-form of hydrosilylated linkage was confirmed according to peak *i* at 2.34 ppm in **Figure 4-1e**. In ^{29}Si NMR spectra, only one peak was observed; this also indicated that there's only β-form formation during hydrosilylation (**Figure 4-2**). The only β-addition product was also obtained by hydrosilylation between silane-monofunctional cyclopentyl or cyclohexyl POSS and

vinyltrimethylsilane.[22] Shockey et al. indicated that the silane functionality might be sterically inaccessible since it is attached directly to the silicon-oxygen framework of the POSS cage and could therefore be shielded by the adjacent cyclic alkyl groups.[22] In our study, two bulky pyrene rings also play an important role in the sterically favorable β-addition product. In MALDI-TOF mass spectrum, the monodispersity at 1441.40 g/mol of BPy-POSS Ag^{+}-complex can be detected (**Figure 4-3**) in agreement with the theoretical value of 1441.37 g/mol.[81,90-91,94-95]

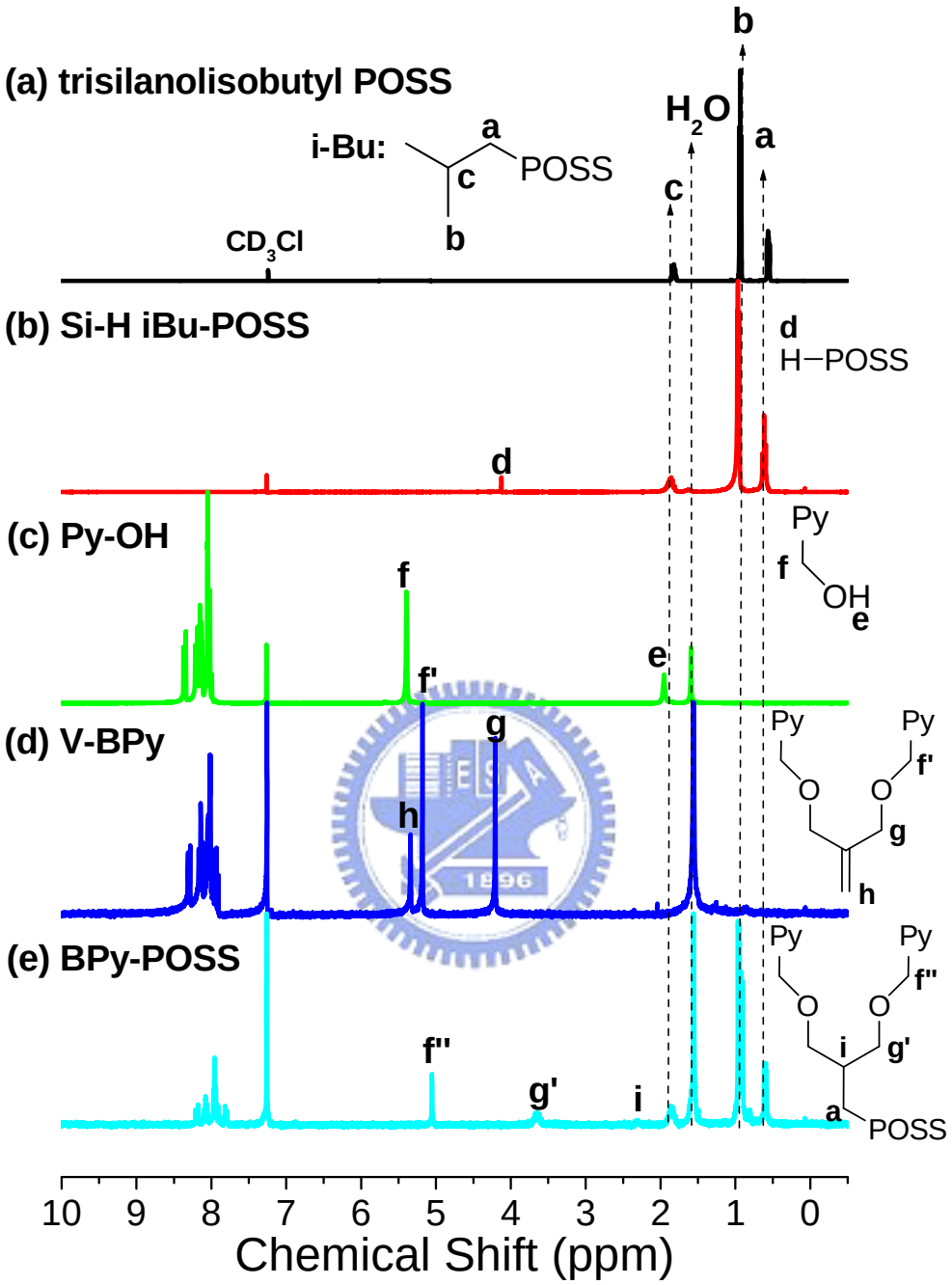

Figure 4-1. ^{1}H NMR spectra of (a) trisilanolisobutyl POSS, (b) Si-H iBu-POSS, (c) Py-OH, (d) V-BPy, and (e) BPy-POSS.

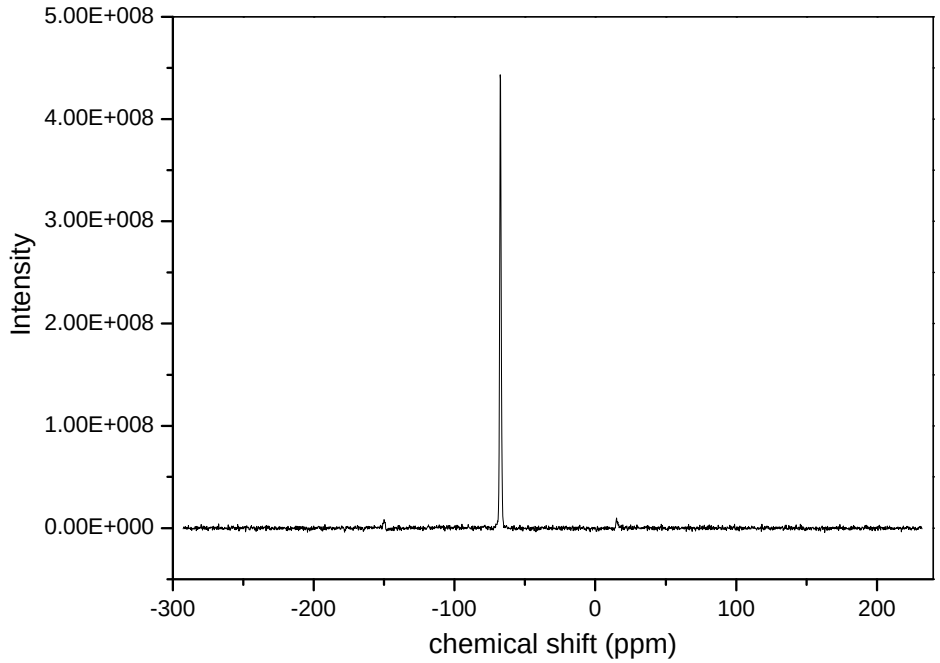

Figure 4-2. ^{29}Si NMR spectra of BPy-POSS.

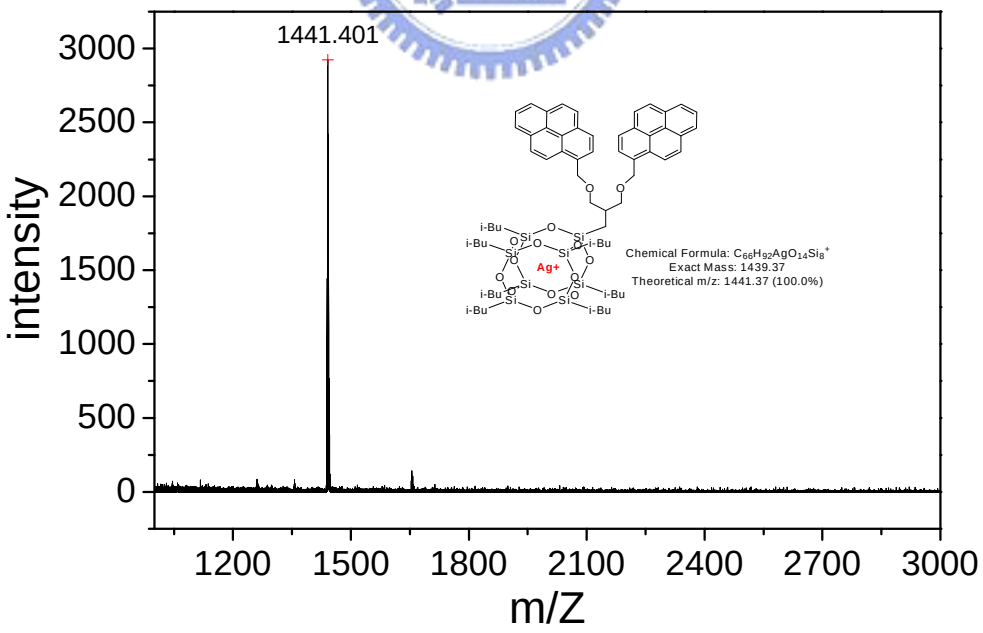

Figure 4-3. MALDI-TOF mass spectrum of BPy-POSS.

4.2 Character of BPy-POSS

4.2.1 Thermal properties

The thermal decomposition temperature (T_d) is 307.90 °C using thermal gravimetric analysis (TGA). Other thermal properties are determined by differential scanning calorimeter (DSC). Highly symmetric T8-POSSes with alkyl chains on a siloxane cube can form a molecule-like crystal.[14] To compare with crystal i-Bu POSS (T_m at 56.0 °C) and amorphous V-BPy (T_g at 14.6 °C), the product of β-hydrosilylated BPy-POSS was a semicrystal solid with crystal POSS domains and amorphous bispyrenyl domains, corresponding to temperatures of glass transition (T_g), recyrstallization (T_c), and melting (T_m) at 14.2, 62.7, and 127.7 °C in **Figure 4-4**. In cooling process, the BPy-POSS can not crystallize perfectly because of the steric hindrance of bispyrenyl group. When heating again beyond the T_g of BPy-POSS, it will rearrange and result in a recrystallization peak. It is notable that the two pyrene rings hinder BPy-POSS from crystallization of POSS moiety, resulting in a higher, polymer-like, broad melting point at 127.7 °C.

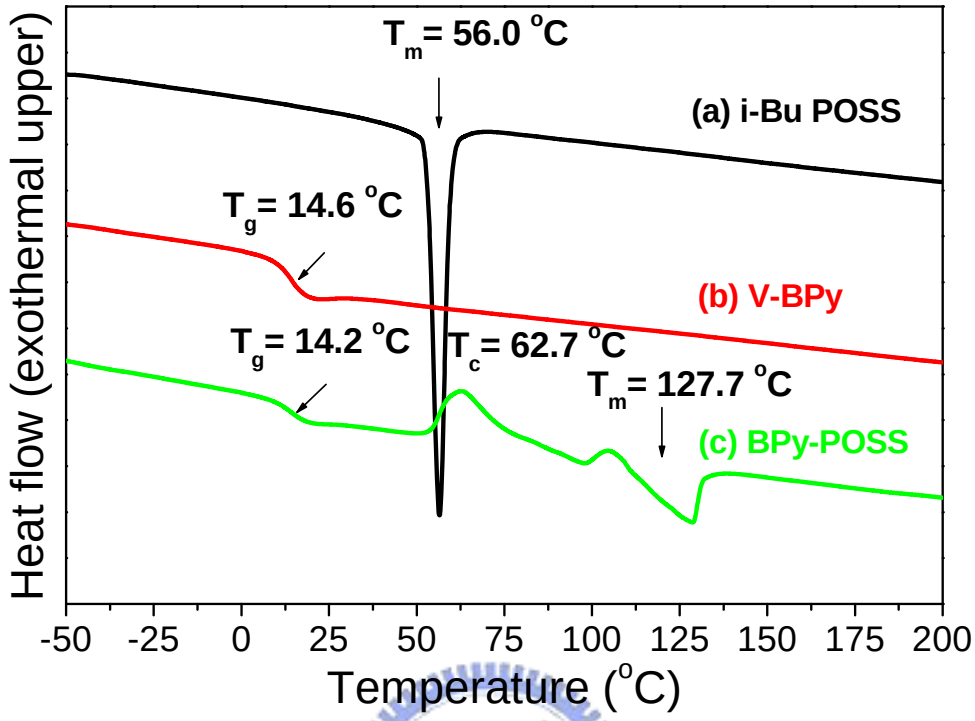

Figure 4-4. DSC thermograms of (a) i-Bu POSS, (b) V-BPy, and (c) BPy-POSS.

4.2.2 Transmission Electronic Microscopy (TEM)

The typical TEM image of the ultra-thin film of BPy-POSS shows about 3-5 nm-width dark fibers of POSS-moiety crystal regions in **Figure 4-5** by electron scattering on silicon atoms.[17-18,24] Herein, the crystal fractal morphology can be observed in TEM image, indicating that BPy-POSS is a semi-crystal material, which is consistent with the DSC data.

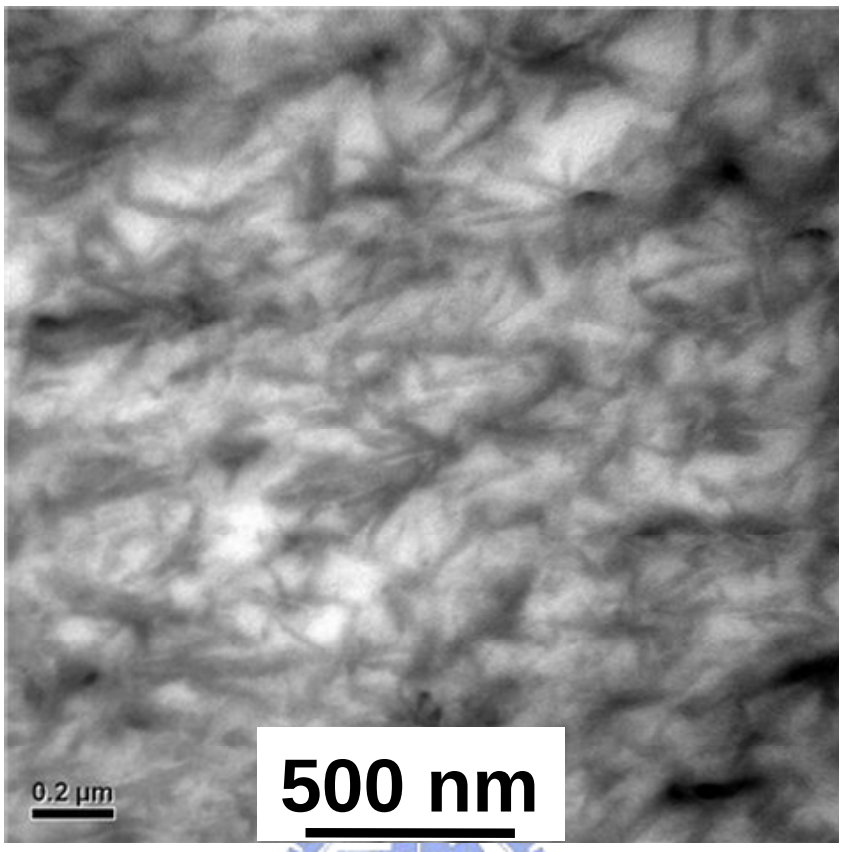

Figure 4-5. Bright-field TEM micrograph for a thin section of BPy-POSS without stained.

4.2.3 UV-Vis and PL Spectroscopy

The chemical structures of V-BPy and BPy-POSS are similar to butterflies. The flexible ether linkages between pyrene rings and POSS moiety result in two conformational isomers of enthalpy-favor close form and entropy-favor open form as shown in **Figure 2-1**. For UV-Vis and PL spectroscopic studies, the uniform and transparent thin films of Py-OH, V-BPy and BPy-POSS were fabricated through spin coating process.

Before investigating the role of the pyrene in the photoluminescent analyses, we need to analyze the effect of the discrepancy between chemical structures of Py-OH, V-BPy, and BPy-POSS have little effect upon the UV-absorbance of pyrene functional groups. As shown in **Figure 4-6**, the UV-Vis absorption spectra of the

V-BPy and BPy-POSS in dilute solution (dichloromethane, 10^{-5} M) are very similar to that of Py-OH. These peaks at 313.4, 327.6, and 344.0 nm indicate that there is coupling of the vibronic features corresponding to the transitions from ν=0 to ν'= 0, 1, 2, where ν and ν' are the quantum vibrational numbers of the ground and excited states, respectively.[67] The photoluminescent spectra of dichloromethane solutions (10^{-5} M) of Py-OH, V-BPy, and BPy-POSS excited by light source with wavelength of 343 nm are shown in **Figure 4-7**. The spectra of the Py-OH monomers without excimer emission (470.7 nm) showing two strong sharp bands at 378.8 and 398.0 nm and two additional shoulder bands at 416.5 and 446.8 nm are almost the same as those of monofunctional pyrene because it is well-dispersed within solvent.[81,67,108] The spectrum of the bispyrenyl V-BPy solution shows the enthalpy-favor result with two relatively weak emission bands of pyrene monomers (open form) at 378.8 and 398.0 nm similar to Py-OH and exhibits a strong typical excimer emission (close form) at 470.7 nm.[62,81,67,108-109] The emission intensity ratio of the excimer band to the monomer band ($I_{470.7}/I_{378.8}$) was calculated to be about 5.2. It is notable that the excimer emission of V-BPy close forms results from intramolecular pyrene-pyrene stacking (π-π interaction) through the thermal rotation of flexible ether linkages. In contrast, the spectrum of the BPy-POSS solution shows result of two relatively strong emission bands of pyrene monomers at 385.5 and 404.2 nm which are red-shifted about 6.5 nm from that of Py-OH or V-BPy because of the effect of POSS moiety, and additionally exhibits a medium typical excimer emission at 470.7 nm.[62,81,67,108-109] The emission intensity ratio of the excimer band to the monomer band ($I_{470.7}/I_{385.5}$) was reduced to be about 0.63. Kim et al[108] indicated that as the size of the aggregate of pyrene-monofunctional compounds increased, the emission shifted toward the higher wavelengths in accordance with the previous experimental and theoretical works that face-to-face stacking interactions in aromatic π-systems resulted in an

increase in the intensity of the transitions and in turn led to a red shift of photoluminescence spectra.[110-111] Herein, colloidal POSS moieties tend to dynamic aggregation, inducing the change in the photoluminescence spectra that conformation isomers with excimer at 470.7 nm, monomer emission at 385.5 and 404.2 nm. The monomer emission of BPy-POSS came along with the intermolecular excimer due to the steric hindrance arising from the aggregation of bulk POSS moieties, which can be observed by DLS. One BPy-POSS possesses two pyrene rings; when one pyrene ring associates with a pyrene ring of other BPy-POSS, the other pyrene ring could be steric hindered then they can not have inter- and intra- associated with other pyrene rings, thus the monomer emission of PL spectra was observed at 385.5 and 404.2 nm. **Figure 4-8** illustrates PL spectra of thin films of V-BPy and BPy-POSS were annealed at 150 °C. In the spectrum of annealed V-BPy thin film, the monomer emission at 396.5, 418.9 and 444.7 nm appeared due to ether bond rotation; and there are still a strong excimer emissions at 473.7 nm and 500.3 nm. In the spectrum of annealed BPy-POSS thin film, the shape remains as the same as pristine thin film does, indicating that the POSS moiety hindered the rotation of ether bond and the packing of BPy-POSS is stable.

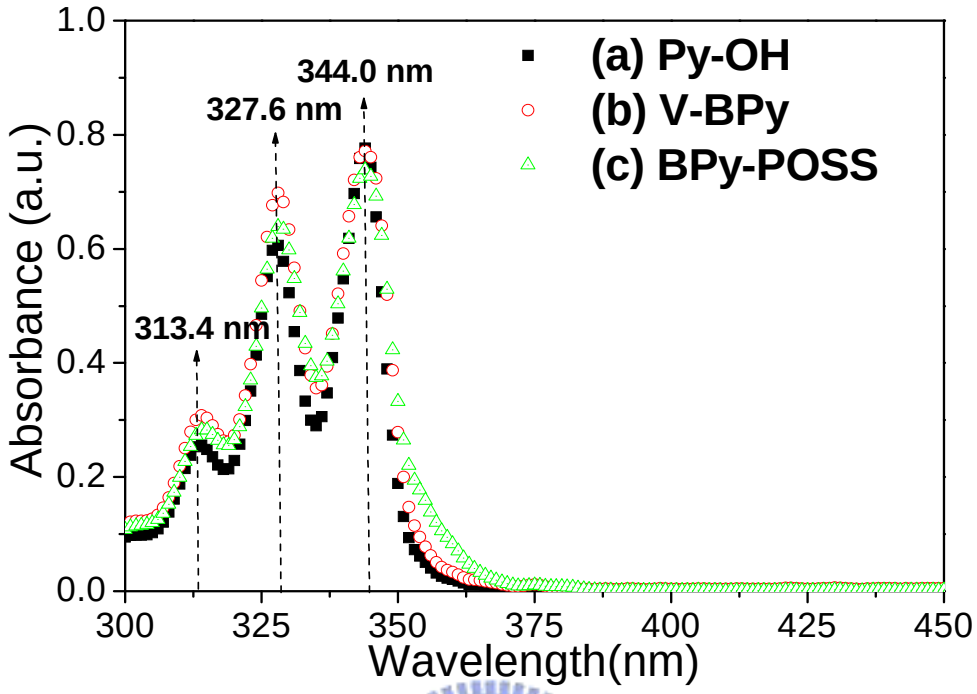

Figure 4-6. UV-Vis spectra of dichloromethane solutions (10^{-5} M) of (a) Py-OH, (b) V-BPy, and (c) BPy-POSS.

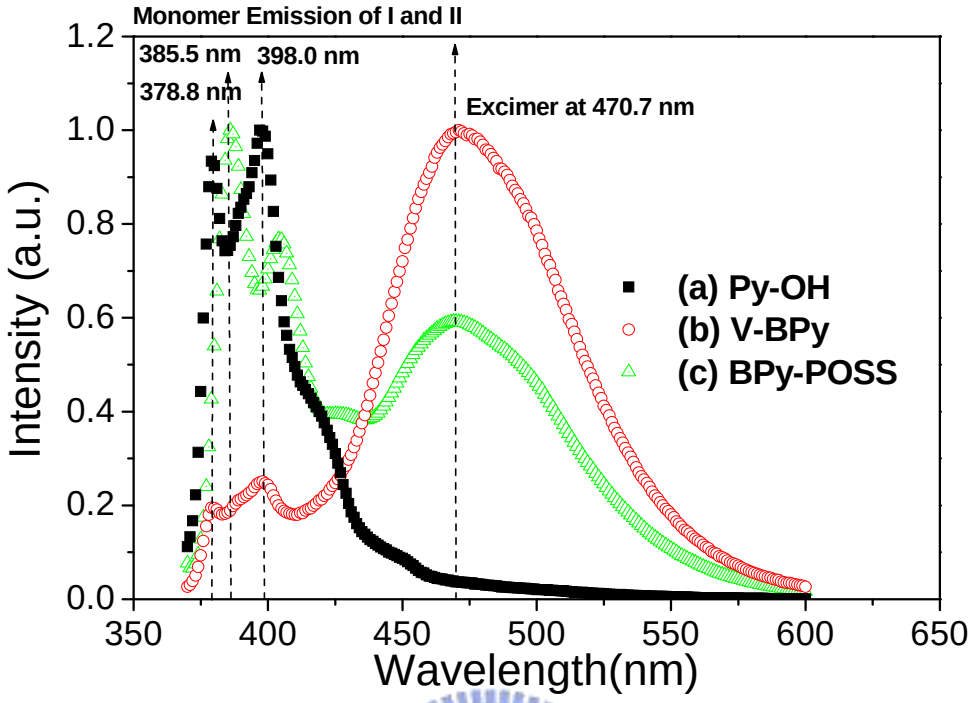

Figure 4-7. Normalized emission and excitation spectra of dichloromethane solutions (10^{-5} M) of (a) Py-OH, (b) V-BPy, and (c) BPy-POSS.

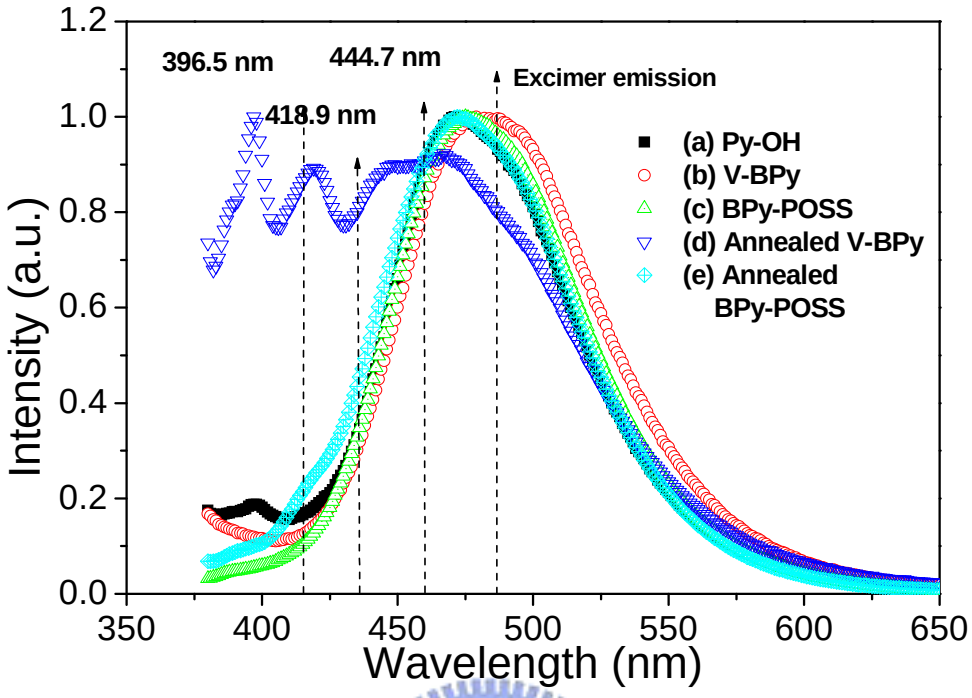

Figure 4-8. Normalized emission and excitation spectra of thin film samples of (a) Py-OH, (b) V-BPy, (c) BPy-POSS, (d) thermal annealed V-BPy, and (e) thermal annealed BPy-POSS.

4.2.4 Dynamic Light Scattering (DLS)

Lu et al. used CS Chem 3D software (MM2 calculations) for molecular modeling to calculate the cubic size of POSS (ca. 0.53 nm); the same method was used to calculate the length of isobutyl groups (ca. 0.43 nm) (**Figure 4-9**). The data show that the diameter of i-Bu POSS without aggregation is about 1.4 nm. As shown in **Figure 4-10**, the average diameter of these aggregations is about 3.72 nm. This indicates that i-Bu POSS exists in a form of slight aggregation in the toluene solution. Comparing to i-Bu POSS, Chem 3D software calculates the diameter of bispyrenyl group about 1.213 nm, and the diameter of BPy-POSS is about 2.17 nm. The DLS data of BPy-POSS indicates that there's a large aggregation in the toluene solution; the average diameter

of these large aggregation is about 22.4 nm (**Figure 4-11**). The reason of forming BPy-POSS aggregation is the aggregation of POSS colloid and the inter- and intra-π-π stacking of pyrene rings.

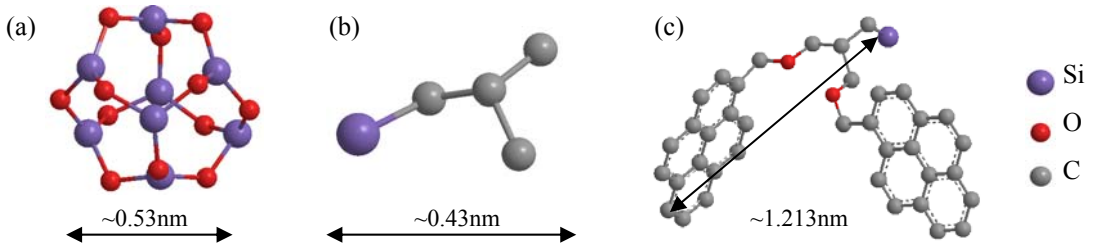

Figure 4-9. Chem 3D MM2 calculations and 3D structures of (a) a POSS core, (b) the iso-butyl group of i-Bu POSS, (c) bispyrenyl group of BPy-POSS.

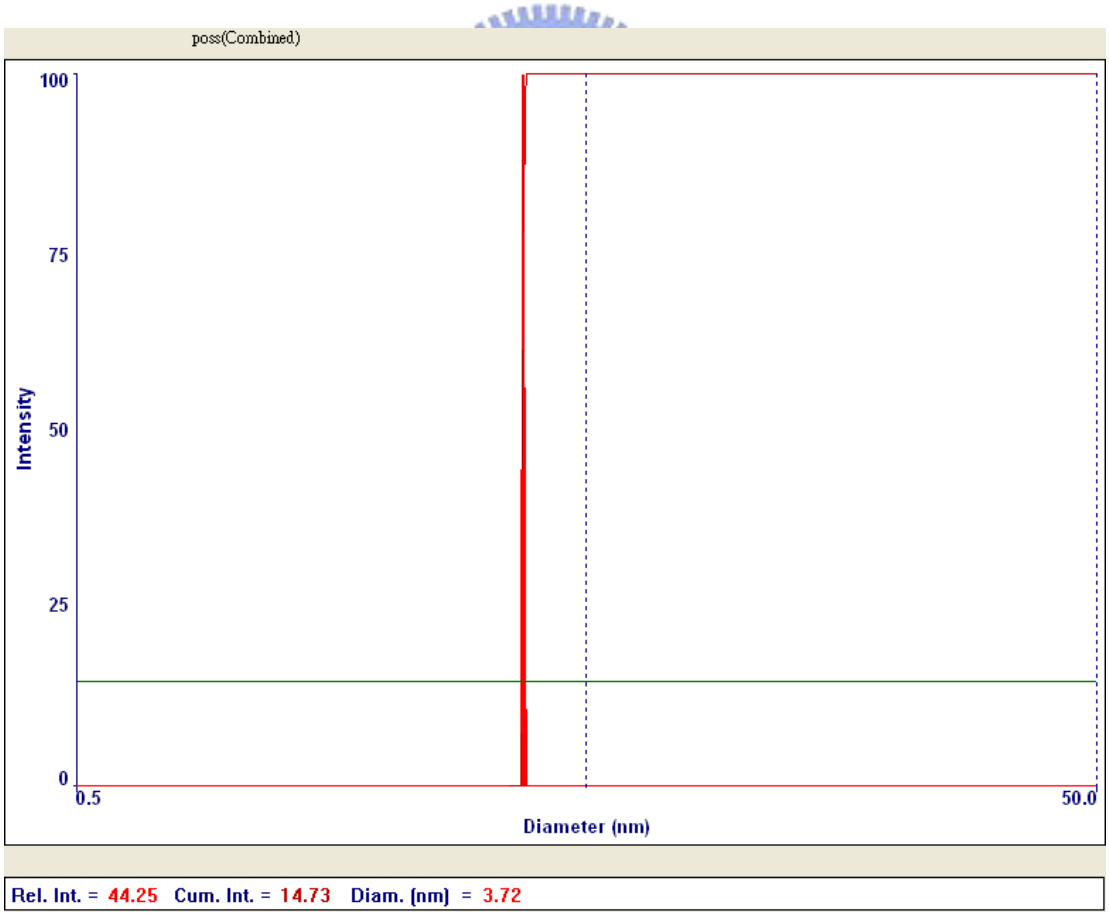

Figure 4-10. Particle distribution of i-Bu POSS by DLS.

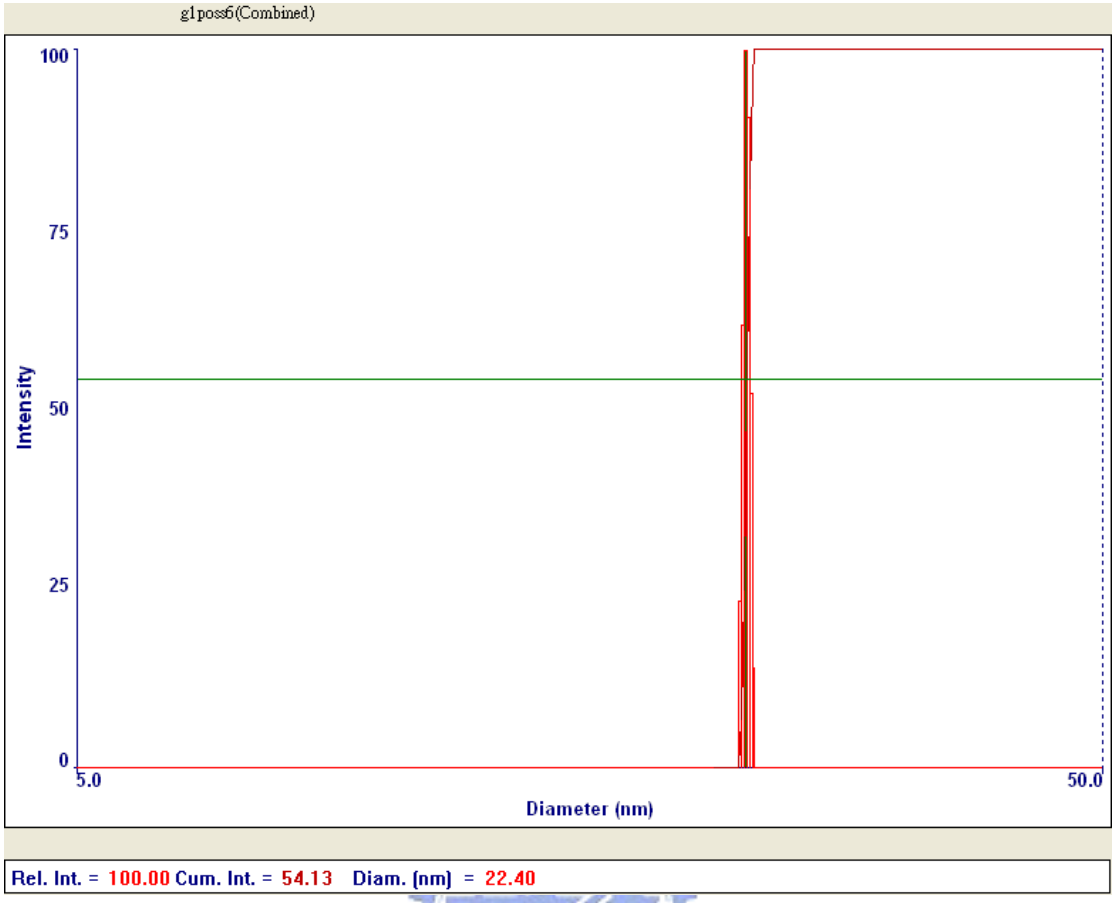

Figure 4-11. Particle distribution of BPy-POSS by DLS.

4.3 Microstructure of Blends

In our previous work, we used thiol-monofunctional isobutyl POSS (SH-POSS) to stabilize gold nanoparticles (POSS-Au NPs) and found that excess SH-POSS can form a fernlike template for incorporation of POSS-Au NPs on its surface through POSS-POSS recognition.[15] In addition, we found that the fernlike crystal microstructures are produced on the interface between a solid supporter, liquid solution, and air so that we can easily prepare a POSS template by advancing and receding process (**Scheme 4-1**). Thus, we can blend BPy-POSS with iBu-POSS to give a photoluminescent thin film with surface pyrene-anchored groups. Herein, pure i-Bu POSS, blends II, blned III and pure BPy-POSS are indicative of the mixtures of BPy-POSS with the weight fractions of i-Bu POSS at 100, 80, 95, and 0 wt% (**Table 4-1**).

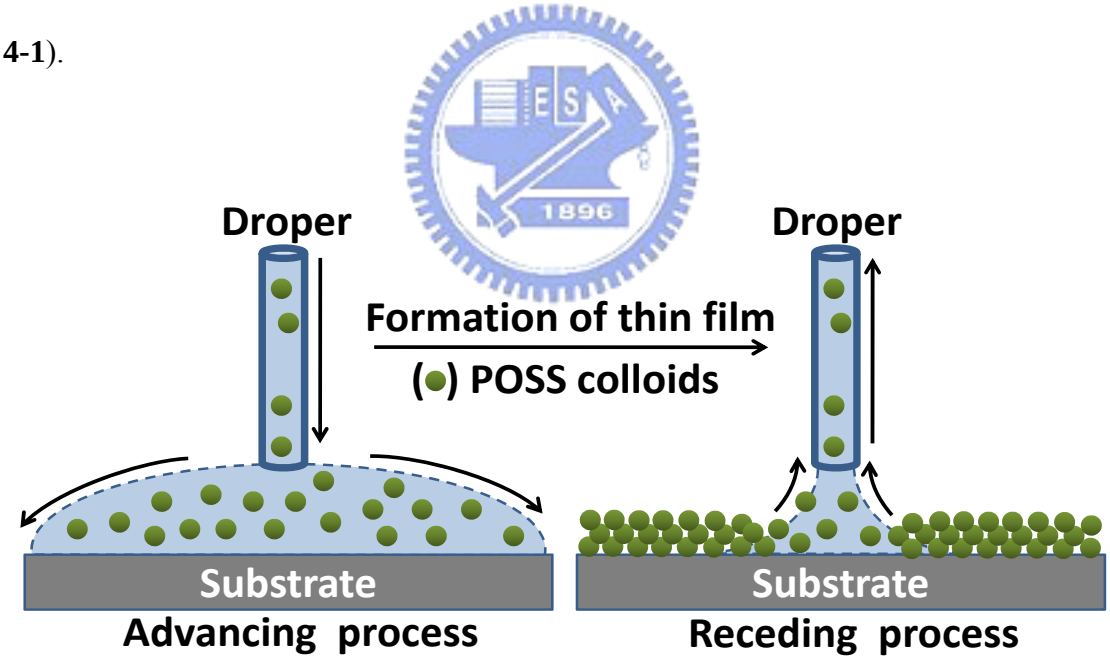

Scheme 4-1. Formation of crystal POSS thin film through advancing and receding process.

Table 4-1. Compositions of pure i-Bu POSS, blend II, blend III and pure BPy-POSS.

	i-Bu POSS (wt%)	BPy-POSS (wt%)
Pure i-Bu POSS	100	0
Blend Ⅱ	95	5
Blend Ⅲ	80	20
Pure BPy-POSS	0	100

4.3.1 Microscopy

4.3.1.1 Confocal Microscopy

As shown in **Figure 4-12a-I**, the fernlike fractal of 100 wt% i-Bu POSS crystals (pure i-Bu POSS) can be observed by optical microscopy.[15,112] Comparably, we didn't observe the similar fractals for pure BPy-POSS in **Figure 4-12a-IV**, probably due to steric hindrance of amorphous bispyrenyl group; the steric hindrance of bispyrenyl group suppresses the crystallization of POSS moiety of BPy-POSS then result in no fernlike structure observed. Photoluminescent images of blends II and III show the bright fernlike fractals labeled with fluorescent bispyrene groups in **Figures 4-12b-II** and **Figure 4-12b–III**, respectively. In comparison with the blend II, the more narrow width and the denser distribution of fractals are shown for the blend III because of the suppression of i-Bu POSS vertical crystallization while BPy-POSS molecules are absorbed onto the surface of i-Bu POSS crystals.[15] In addition, the superimposed images of blends II and III clearly showed that fluorescent bispyrene groups are located in the region of fernlike fractals in **Figure 4-12c-II** and **Figure 4-12c-III**.

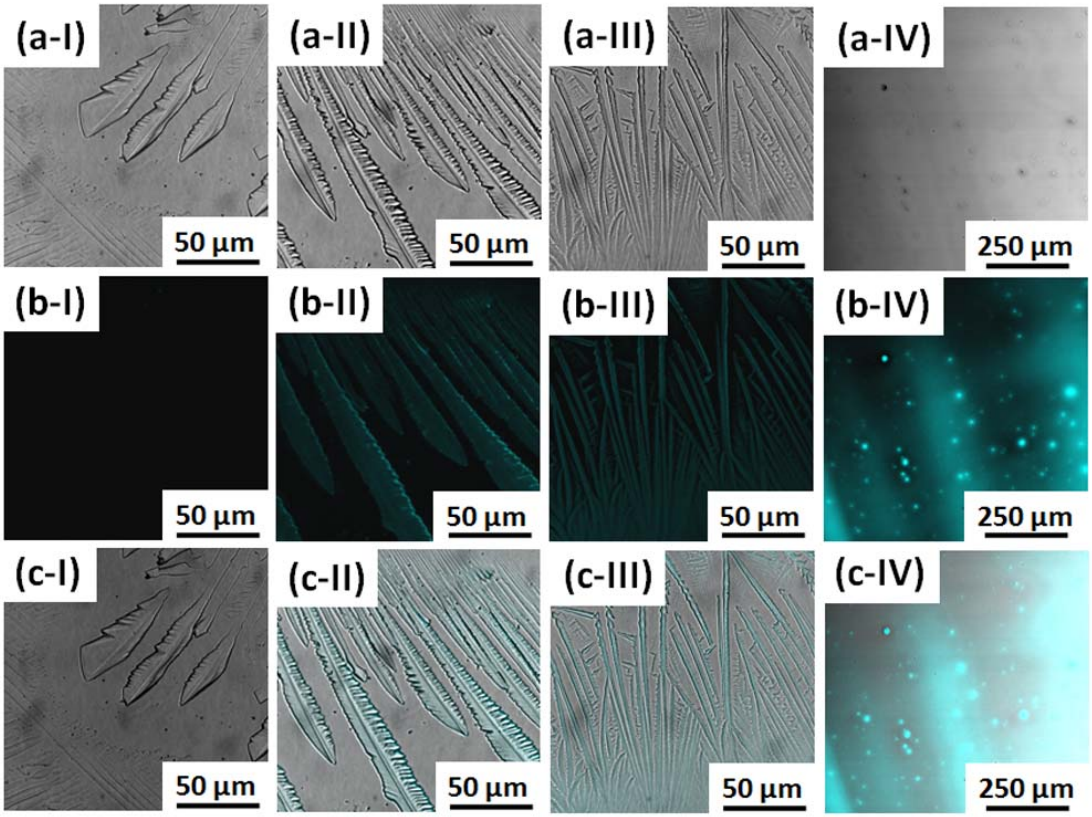

Figure 4-12. (a) OM images, (b) PL images, and (c) their superimposed images for thin-film of i-Bu POSS, blend II, blend III and BPy-POSS.

4.3.1.2 Atomic Force Microscopy (AFM)

AFM analyses (sectional analyses and 2D images) revealed similar fernlike microstructures in confocal microscopy of blends II and III (**Figure 4-13a** and **4-13b**), similar to those of POSS-Au hybrid nanoparticles in our previous study.[15] The fernlike microstructures of blends II and III were ca. 2.93 and 3.75 μm wide; the detected tapes heights were 198.30 and 140.87 nm, respectively. In comparison, AFM image of blend III is rougher than the AFM image of blend II. The rough surface of blend III is caused by the excess BPy-POSS molecules for blends III aggregated on the surface of i-Bu POSS crystals.

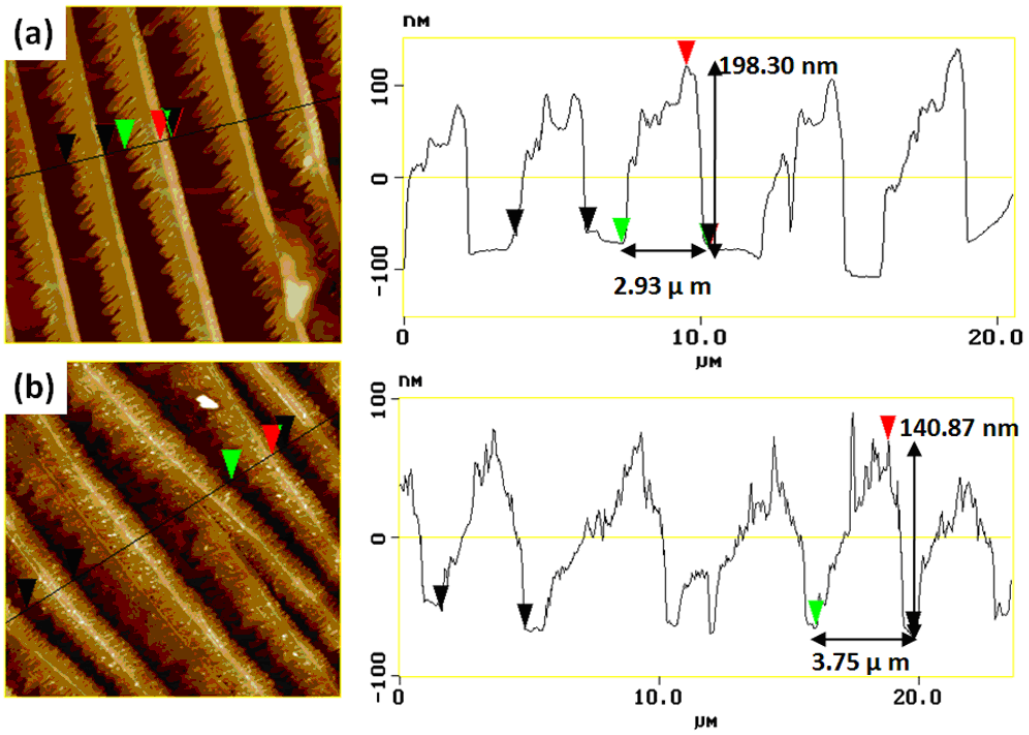

Figure 4-13. AFM 2D images and sectional analyses of (a) blend II and (b) blend III with scale of 20× 20 μm^2.

4.3.2 X-Ray Powder Diffraction

The X-ray diffraction patterns of thin-film blends are shown in **Figure 4-14**. Spectrum of pure i-Bu POSS shows several characteristic peaks (2θ= 7.91°, 8.85°, 17.81°, 26.84°) of i-Bu POSS.[113-114] In the XRD patterns of blend II, the small amount of BPy-POSS molecules (5%) can be well-dispersed onto the surface of the i-Bu POSS crystal fernlike template without BPy-POSS aggregation through the association between POSSs, thus the pattern of blend II is similar to that of pure i-Bu POSS. [15,115] The broad signals of blend III and pure BPy-POSS centered at 20° are indicative of the existence of amorphous aggregation of bispyrene domains (**Figure 4-14c** and **4-14d**), which is in agreement with the glass transition of BPy-POSS at 14.2 °C (**Figure 4-4c**). As the content of BPy-POSS was increased up to 20 wt%, the broad halo in spectra of blend III and pure BPy-POSS centered at 20° occurred

because of the formation of slight aggregation of BPy-POSS on the surface of i-Bu POSS crystal fernlike template. The peak at 2θ=5.76° was corresponded to the d-spacing of 1.53 nm and the calculated size of bispyrenyl group we calculated was 1.31 nm, suspecting the presence of the aggregated and arranged bispyrenyl domain.

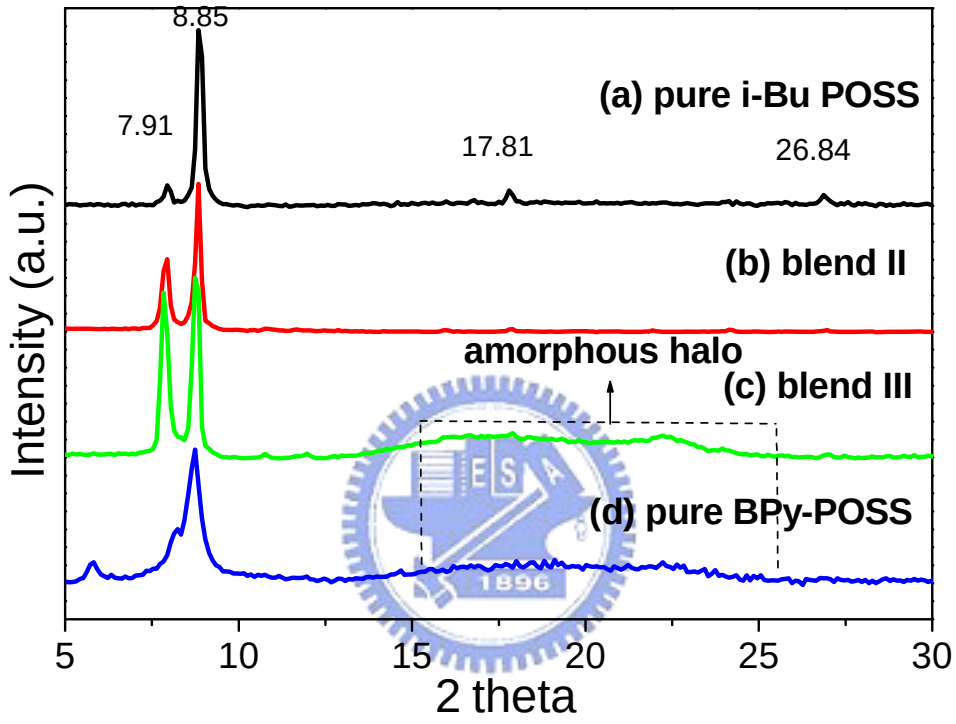

Figure 4-14. XRD spectra of thin-film Samples.

4.3.3 Differential Scanning Calorimeter (DSC)

In the studies by Cui et al,[17] they prepared a 3,6,7,10,11-pentakis(pentyloxy)triphenylene-monofunctional POSS (P5T-POSS), exhibiting a spacer about 16-carbon length and found that the co-crystallization of P5T-POSS and i-Bu POSS were able to afford a sandwich-like microstructure with single melting point. Herein, the space length of BPy-POSS is relatively shorter so that the steric hindrance of bispyrene units would become significant and influence

the crystallization of POSS units resulting in polymer-like recrystallization at 62.7 °C and higher melting points at 127.7 °C as shown in the DSC thermogram (**Figure 4-4c**). Thus, we suspected that semicrystal BPy-POSS would phase-separate from i-Bu POSS crystal domain and then, two melting points at 53.6 °C and 122.0 °C were observed in the DSC thermogram of blend III with 20 wt% BPy-POSS (**Figure 4-15b**). With increasing the composition of BPy-POSS up to 50 wt%, the melting point at 122.0 °C and the glass transition temperature at 23.7 °C became apparent in the heating DSC thermogram which indicated the presence of the phase separation of i-Bu POSS and BPy-POSS (**Figure 4-15c**). Therefore, we can concluded that BPy-POSS with a bulk bispyrene units can self-assemble (POSS-POSS recognition) onto the surface of i-Bu POSS crystal template to obtain a surface-enriched bispyrene fernlike thin film.

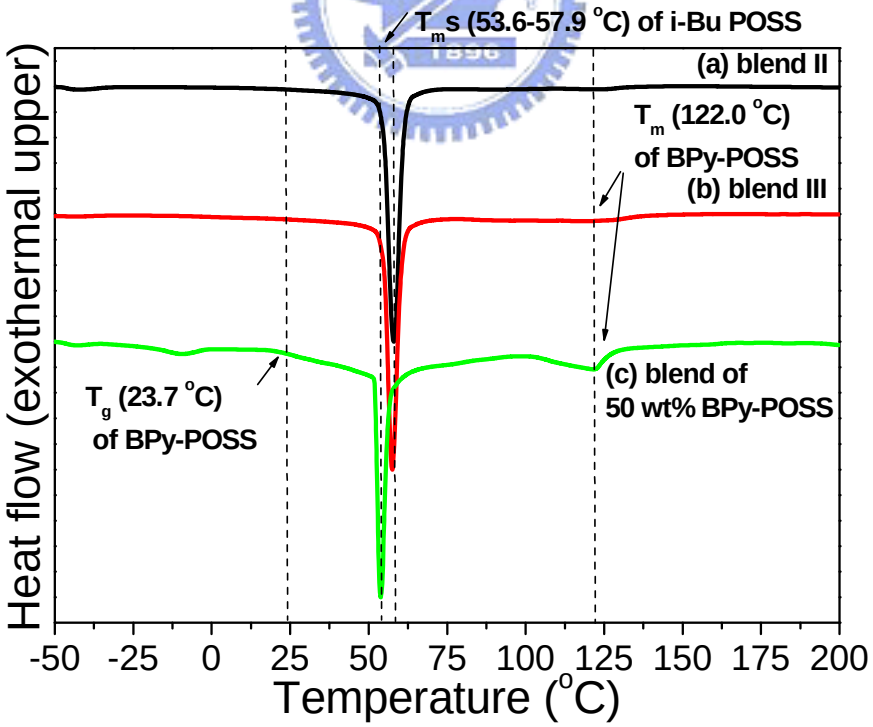

Figure 4-15. DSC thermograms of blends (a) II, (b) III, and (c) 50 wt% BPy-POSS and 50 wt% i-Bu POSS.

4-4 Application in Chemosensor

PL fernlike patterns of blends II and blend III observed in **Figure 4-12b** may be result from the dispersion of BPy-POSS on the surface of i-Bu POSS crystal fractals. In contrast, the pure BPy-POSS tends to form a droplet of concentrate rather than fernlike microstructures. Such an advancing and receding process can be substitute for spin coating because it meets the significant requirement of using small quantities of chromophores in the fabrication of PL thin films as thin as possible. Although these PL fernlike patterns are not uniform as those by spin coating, the spot of the incident beam cover enough chromophores to in-situ monitor the PL response of pyrenyl excimers when PL thin films are exposed to nitrobenzene vapor.

To measure the fluorescence quenching of these thin films with absorption of nitrobenzene using photoluminescence spectra, a specially designed apparatus was employed as shown in **Figure 4-16**. Blend II, blend III and pure BPy-POSS toluene solutions were dropped on the quartz glasses through the advancing and receding process and then placed in a ten-cubic-centimeter plastic box with two quartz windows and one inject hole. When 0.3 ml nitrobenzene was injected into the glass container inside the box through syringe, the PL intensities of pyrenyl excimers for blends II, blend III and pure BPy-POSS at 470 nm were recording for 900s using time scan program under the incident beam at 343 nm. **Figure 4-17, Figure 4-18** and **Figure 4-19** illustrate the fluorescence spectra of blend II, blend III and pure BPy-POSS thin films before and after being treated with nitrobenzene vapor; the decrease in fluorescence intensity at 470 nm is more significant than that at 385 nm (monomer emission) indicated that the nitrobenzene-induced PL quenching is a selective process applying mainly to excimers. The microstructures of BPy-POSS and i-Bu POSS on the thin film surface will affect the interaction between the sensing

element, pyrene, and the quencher, nitrobenzene. In **Figure 4-20**, the quenching efficiencies of three thin films exposing to nitrobenzene vapor were calculated at the emission wavelength of 470 nm; the quenching efficiency was calculated using equation 1

$$\eta = (I_0\text{-}I)/I_0 \times 100\% \quad (1)$$

After injection of nitrobenzene, a period of time was required because nitrobenzene should arrive to the glass container inside the plastic box. In this period of time, the fluorescence quenching efficiency was zero. Most of surface excimer chromophores are rapidly quenched through exposing to the nitrobenzene vapor for 165 s. After about 220 s, the decrease in the absorption of nitrobenzene resulted in a slight increase of quenching efficiency.

It can be observed that the thin film of blend II is more sensitive in absorption of nitrobenzene. Exposing the film to nitrobenzene vapor for 1 min causes ca. 30% quenching of the fluorescence emission, and an additional 60% of the emission was quenched when being exposed for 10 min. Comparing to thin film of blend II, thin film of blend III responded to a lesser degree to nitrobenzene vapor. As observed by AFM topologies and XRD spectra in **Figures 4-13** and **4-14**, we expected that the 5 wt% of BPy-POSS in the blend II can be more efficiently dispersed on the surface of the given POSS templates than the 20 wt% of that in the blend III, so that the more surface excimer chromophores in the blend II exhibits the higher quenching efficiency after 215s as shown in **Figure 4-20**. Comparing with thin film of pure BPy-POSS, the quenching rate of blend II before about 380s is lager than that of pure of BPy-POSS. The reason may be the well dispersion of 5% BPy-POSS in blend II. After 380s, the nitrobenzene vapor diffused into the thin films; the thin film of pure BPy-POSS can absorb nitrobenzene vapor of its nature, but the absorption of nitrobenzene vapor in blend II thin film is approach to saturation.

This result displays the unique property that 5 wt% BPy-POSS is able to be sufficiently dispersed on the surface of 95 wt% i-Bu POSS crystalline fractals for a pyrene-functional chemical sensor to detect nitrobenzene vapor.

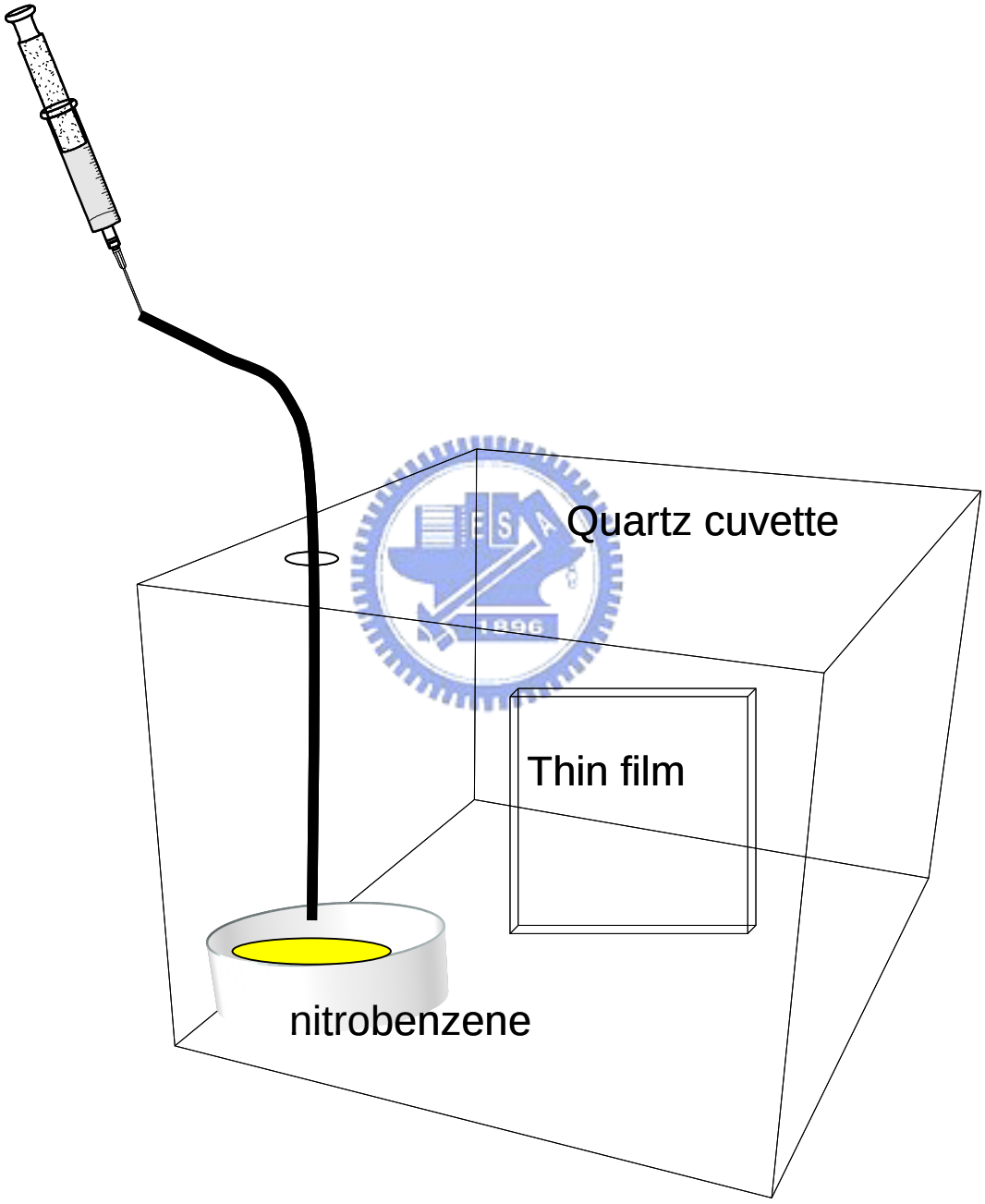

Figure 4-16. Schematics of the designed apparatus.

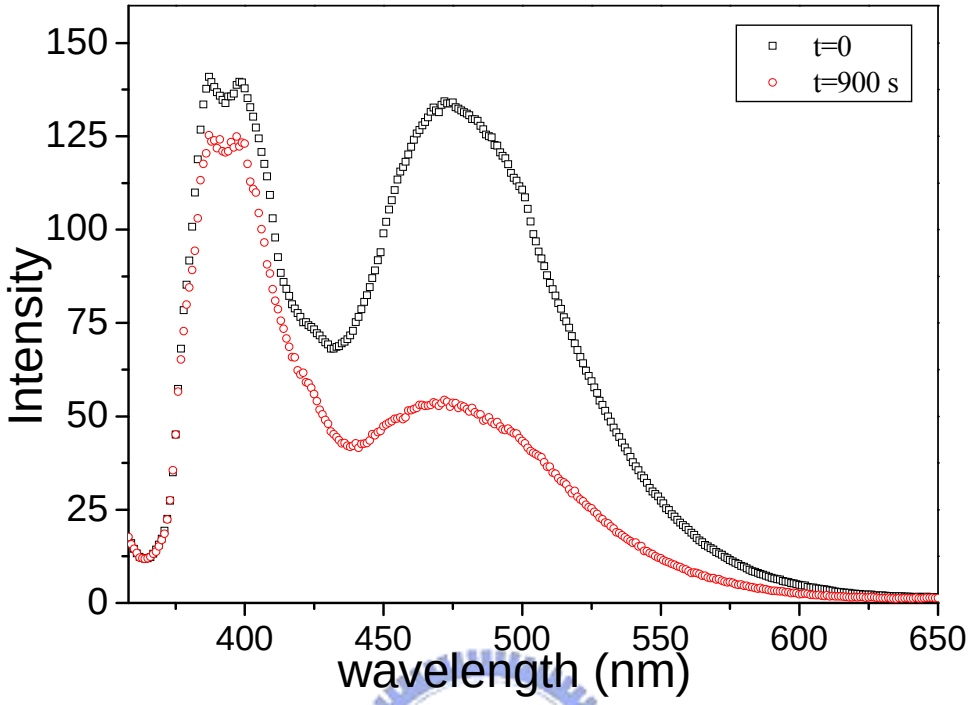

Figure 4-17. Fluorescence spectra of blend II thin film before and after being treated with nitrobenzene vapor.

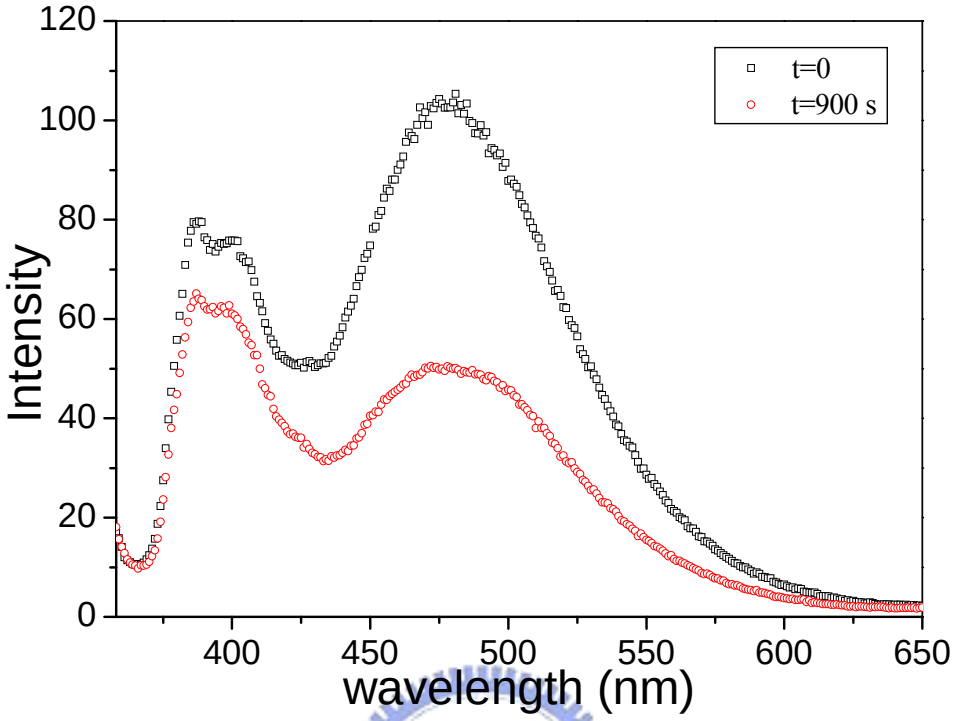

Figure 4-18. Fluorescence spectra of blend III thin film before and after being treated with nitrobenzene vapor.

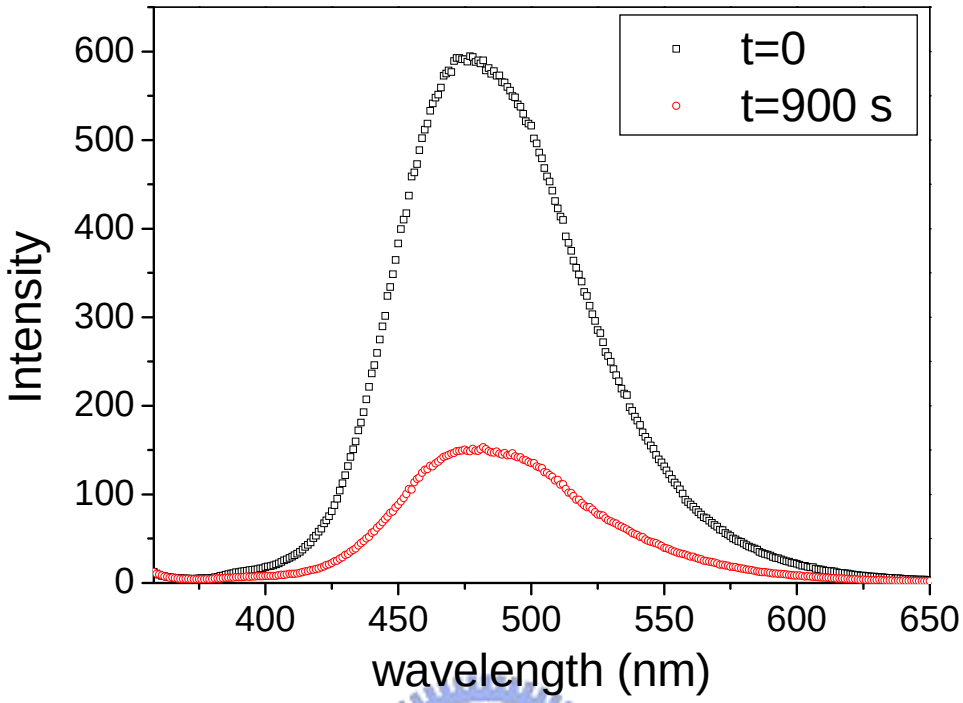

Figure 4-19. Fluorescence spectra of pure BPy-POSS thin film before and after being treated with nitrobenzene vapor.

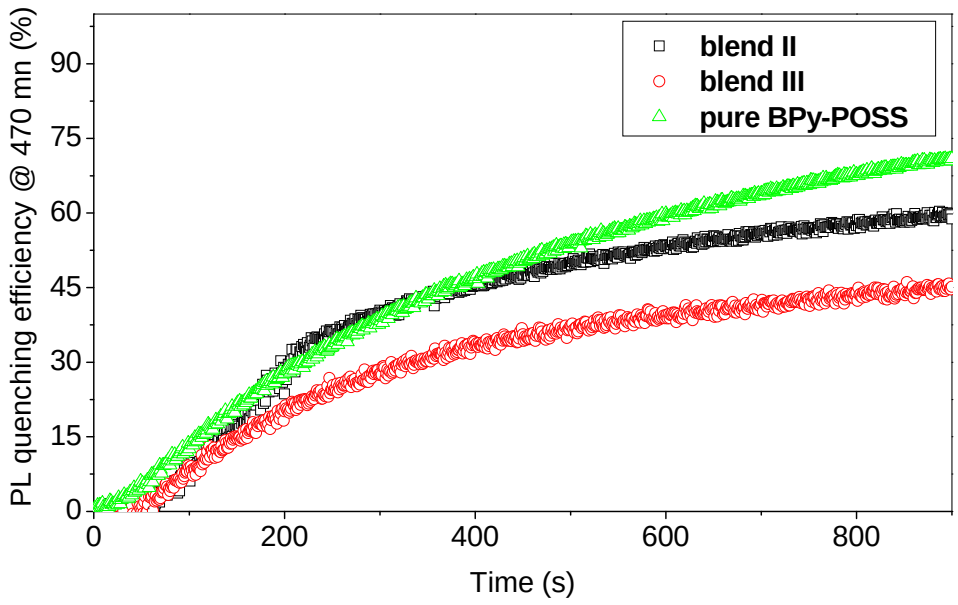

Figure 4-20. Quenching efficiency of nitrobenzene to the fluorescence emission of blend II, blend III and pure BPy-POSS thin films.

Chapter 5

Conclusion

In this study, a bispyrenyl-functional polyhedral oligomeric silsequioxanes (BPy-POSS) was successfully synthesized by hydrosilylation between hydride-monofunctional isobutyl-POSS (Si-H iBu-POSS) and vinyl-functional bispyrene (V-BPy) obtained by etherification of 1-pyrenemethanol (Py-OH) and methallyl dichloride. As characterized by MALDI-TOF mass spectrum, ^{1}H NMR spectrum, DSC thermogram, and solution PL spectrum, as-synthesized BPy-POSS has a monodispersed molar mass distribution at 1441.4 m/z (a complex with Ag ions), only β-hydrosilylated bonds between bipyrenyl and POSS units, a semicrystalline solid composed of amorphous bipyrenyl domains and crystal POSS domains, and a mixture of butterfly-like microstructures with most close open forms.

The phase separation of blends of BPy-POSS and inert isobutyl-POSS (i-Bu POSS) was observed by two glass-transition-temperatures in DSC thermograms and a mixture of crystal and amorphous domains in XRD analyses. As shown in PL microscopic images, the BPy-POSS are well dispersed on the surface of i-Bu POSS crystals to form PL micropatterns closely similar to the fractals of pure i-Bu POSS crystals, which is inactive to the incident UV lights. For a PL sensor in detecting nitrobenzene vapor, the significant decay (20~40%) of pyrenyl excimer emission at 470 nm was observed within 100s. The efficiency of nitrobenzene-induced quenching process for 5% BPy-POSS is higher than that for 20% BPy-POSS. These results indicate the advantage of using i-Bu POSS crystals as a template to disperse BPy-POSS in the capacity improvement of pyrene-based chemical sensors.

Chapter 6

Reference

1. Kickelbick G., *Hybrid materials, synthesis, characterisation and applications*. Wiley-VCH Verlag, 2007, p. 1–48
2. *Hybrid Materials: an Overview*
3. Brett, M. Bode; Paul, N. Day; and Mark, S. Gordon, *J. Am. Chem. Soc.* **1998,** *120,* 1552-1555
4. James, L. Fry; Ronald, J. Rahaim, Jr.; Robert, E. Maleczka, Jr.; *"Triethylsilane", Encyclopedia of Reagents for Organic Synthesis*, John Wiley & Sons, 2007
5. C. Elschenbroich; *Organometallics* (**2006**) Wiley and Sons-VCH: Weinheim. ISBN 978-3-29390-6
6. Marko, I.; Stern, S.; Buisine, O.; Berthon, G.; Michaud, G.; Tinant, B.; Declercq J-P. *Adv. Synth. Catal*. **2004**, *346*, 1429-1434
7. Meads, J. A.; Kipping, F. S. *J. Am. Chem. Soc*. **1915**, *107*, 459.
8. Brown, J. F.; Vogt, L. H. *J. Am. Chem. Soc*. **1965**, *87*, 4313-4317
9. Yuung-Ching Sheen; Chu-Hua Lu; Chih-Feng Huang; Shiao-Wei Kuo; Feng-Chih Chang. *Polymer* **2008**, *49*, 4017-4024
10. L. Kare, *Arkiv for Kemi.* **1960**, *16,* 203
11. Baney, R. H.; Itoh, M.; Sakakibara, A.; Suzuki, T. *Chem. Rev.* **1995**, *95*, 1409-1430
12. Shea, K. J.; Loy, D. A. *Acc. Chem. Res.* **2001**, *34*, 707-716
13. Yamamoto, S.; Yasuda, N.; Ueyama, A.; Adachi, H.; Ishikawa, M. *Macromolecules* **2004**, *37*, 2775-2778
14. Larsson, K. *Ark. Kemi* **1960**, *16*, 209
15. Chu-Hua Lu; Chih-Feng Huang; Shiao-Wei Kuo; Feng- Chih Chang. *J. Phys. Chem. C* **2009**, *113*, 3517-3524

16. Waddon, A. J.; Coughlin, E. B. *Chem. Mater.* **2003**, *15*, 4555-4561

17. Cui, L.; Collet, J. P.; Xu, G.; Zhu, L. *Chem. Mater.* **2006**, *18*, 3503-3512

18. Miao, J.; Cui, L.; Lau, H. P.; Mather, P. T.; Zhu, L. *Macromolecules* **2007**, *40*, 5460-5470

19. Pielichowski, K.; Njuguna, J.; Janowski, B.; Pielichowski. *J. Adv. Polym. Sci.* **2006**, *201*, 225

20. Li, G.; Wang, L.; Ni, H.; Pittman, Jr. C. U. *J. Inorg. Organomet. P.* **2002**, *11*, 123

21. Marcolli, C.; Calzaferrit, G. *Appl. Organometal. Chem.* **1999**, *13*, 213-226

22. Shockey, E. G.; Bolf, A. G.; Jones, P. F.; Schwab, J. J.; Chaffee, K. P.; Haddad, T. S.; Lichtenhan, J. D. *Appl. Organometal. Chem.* **1999**, *13*, 311-327

23. Pan, G. In: Mark, J.E. Editor, *Physical properties of polymers handbook* (2nd ed.), Springer-Verlag, New York, 2006

24. Lichtenhan, J. D.; Haddad, T. S.; Feher, F. J.; Soulivong, D.; U.S. Patent 6,770,724 (**2004)**

25. Tereshchenko, T.A. *Polymer Science Ser. B* **2008**, *50*, 249-262

26. F. J. Feher; D. A. Newman; J. F. Walzer. *J. Am. Chem. Soc.* **1989**, *111*, 1741-1748

27. Feher, F. J.; Weller, K. J. *Inorg. Chem.* **1991**, *30*, 689

28. Lichtenhan, J. D. *Comments Inorg. Chem.* **1995**, *17*, 115

29. María J. Abad; Luis Barral; Diana P. Fasce; Roberto, J. J. Williams. *Macromolecules* **2003,** *36,* 3128-3135

30. J. D. Lichtenhan, J. J. Schwab, F. J. Feher, and D. Soulivong, US Patent No. 5942638 (**1999)**

31. J. D. Lichtenhan; J. J. Schwab; An Y.-Z. et al.; US Patent No. 6911518 (**2005**)

32. Huynh, W. U.; Dittmer, J. J.; Alivisatos, A. P. *Science* **2002**, *295*, 2425-2427

33. Huang, X.; El-Sayed, I. H.; Qian, W.; El-Sayed, M. A. *J. Am. Chem. Soc.* **2006**, *128*, 2115-2120

34. Salem, A. K.; Searson, P. C.; Leong, K. W. *Nat. Mater.* **2003**, *2*, 668-671

35. Patel, A. C.; Li, S.; Wang, C.; Zhang, W.; Wei, Y. *Chem. Mater.* **2007**, *19*, 1231-1238

36. Glotzer, S. C.; Solomon, M. J. *Nat. Mater.* **2007**, *6*, 557-562

37. Love, J. C.; Urbach, A. R.; Prentiss, M. G.; Whitesides, G. M. *J. Am. Chem. Soc.* **2003**, *125*, 12696-12697

38. Salant, A.; Amitay-Sadovsky, E.; Banin, U. *J. Am. Chem. Soc.* **2006**, *128*, 10006-10007

39. Mokari, T.; Rothenberg, E.; Popov, I.; Costi, R.; Banin, U. *Science* **2004**, *304*, 1787-1790

40. Caswell, K. K.; Wilson, J. N.; Bunz, U. H. F.; Murphy, C. J. *J. Am. Chem. Soc.* **2003**, *125*, 13914-13915

41. Jackson, A. M.; Myerson, J. W.; Stellacci, F. *Nat. Mater.* **2004**, *3*, 330-336

42. Roucoux, A.; Schulz, J.; Patin, H. *Chem. Rev.* **2002**, *102*, 3757-3778

43. Petit, C.; Taleb, A.; Pileni, M. P. *Adv. Mater.* **1998**, *10*, 259-261

44. Murray, C. B.; Kagan, C. R.; Bawendi, M. G. *Annu. Rev. Mater. Sci.* **2000**, *30*, 545-610

45. Andres, R. P.; Bielefeld, J. D.; Henderson, J. I.; Janes, D. B.; Kolagunta, V. R.; Kubiak, C. P.; Mahoney, W. J.; Osifchin, R. G. *Science*, **1996**, *273*, 1690-1693

46. Markovich, G. *Acc. Chem. Res.* **1999**, *32*, 415-423

47. Liu, J. *J. Am. Chem. Soc.* **1999**, *121*, 4340-4347

48. Marinakos, S. M.; Brousseau, L. C., III; Jones, A.; Feldheim, D. L. *Chem. Mater.* **1998**, *10*, 1214-1219

49. Whettern, R. L. *Acc. Chem. Res.* **1998**, *31*, 397-404

50. Boal, A. K.; Iihan, F.; DeRouchey, J. E.; Thurn-Albrecht, T.; Russell, T. P.; Rotello, V. M. *Nature* **2000**, *404*, 746-748

51. Li, B.; Ni, C.; Li, C. Y. *Macromolecules* **2008**, *41*, 149-155

52. Wang, G.; Murray, R. W. *Nano Lett.* **2004**, *4*, 95-101

53. Shenhar, S.; Rotello, V. M. *Acc. Chem. Res.* **2003**, *36*, 549-561

54. Sato, T.; Hasko, D. G.; Ahmed, H. *J. Vac. Sci. Technol.* **1997**, *B15*, 45

55. Lin, X. M.; Pathasarathy, R.; Jaeger, H. M. *Appl. Phys. Lett.* **2001**, *78*, 1915-1917

56. Larsson, K. *Ark. Kemi* **1960**, *16*, 203

57. Sloog, Holler, Nieman, Principles of instrumental anaylsis, fifth addition.

58. Xu, W.; Schmidt, R.; Whaley, M.; Demas, J. N.; DeGraff, B. A.; Karikari, E. K.; Famer, B. A. *Anal. Chem.* **1995**, *67*, 3172-3180

59. Zhang, S. J.; Lü, F. T.; Gao, L. N.; Ding, L. P.; Fang, Y. *Langmuir* **2007**, *23*, 1584-1590

60. Fujiwara, Y.; Okura, I.; Miyashita, T.; Amao, Y. *Anal. Chim. Acta* **2002**, *471*, 25

61. Bai, H.; Li, C.; Shi, G. Q. *Sens. Actuators B* **2008**, *130*, 777-782

62. Karpovich, D. S.; Blanchard, G. J. *J. Phys. Chem.* **1995**, *99*, 3951-3958

63. Isadore B. Berlman, Handbook of fluorescence spectra of aromatic molecules, second edition, New York and London.

64. P. Hammarstroëm et al, *FEBS Letters*, **1997**, *420*, 63-68

65. Foë rster, T. *Angew. Chem. Int. Ed*, **1969**, *8*, 333

66. Birks, J. B, *Rep. Prog. Phys.,* **1975**, *38*, 903

67. Winnik, F. M. *Chem. Rev.* **1993**, *93*, 587-614

68. de Silva, A. P.; Gunaratne, H. Q. N.; Gunnlaugsson, T.; Huxley, A. J. M.; McCoy, C. P.; Rademacher, J. T.; Rice, T. E. *Chem. Rev.* **1997**, *97*, 1515-1566

69. Desvergne, J.-P.; Czarnik, A. W., Eds.; NATO ASI Ser.; Kluwer Academic; Dordrecht, *Chemosensors of Ion and Molecule Recognition*; The Netherlands, 1997; p 492.

70. Valeur, B.; Leray, I. *Coord. Chem. Rev.* **2000**, *205*, 3-40

71. Fabbrizzi, L.; Poggi, A. *Chem. Soc. Rev*. **1995**, *24*, 197-202

72. (a) Nohta, H.; Satozono, H.; Koiso, K.; Yoshida, H.; Ishida, J.; Yamaguchi, M. m *Anal. Chem*. **2000**, *72*, 4199-4204

(b) Okamoto, A.; Ichiba, T.; Saito, I. *J. Am. Chem. Soc*. **2004**, *126*, 8364-8365

73. Birks, J. B. *Photophysics of Aromatic Molecules*; Wiley-Interscience: London, 1970.

74. Sung Kuk Kim, Seoung Ho Lee, Ji Yeon Lee, Jin Yong Lee, Richard A. Bartsch, Jong Seung Kim, *J. Am. Chem. Soc*. **2004**, *126*, 16499-16506

75. Hideya Yuasa,* Naofusa Miyagawa, Takuhiro Izumi, Masatoshi Nakatani, Masayuki Izumi, and Hironobu Hashimoto, *Org. Lett.*, **2004**, *6*, 1489-1492

76. Zhuo Wang; Deqing Zhang; Daoben Zhua, *Analytica Chimica Acta,* **2005,** *549*, 10-13

77. Benjamin Schazmann; Nameer Alhashimy; Dermot Diamond, *J. Am. Chem. Soc.*, **2006**, *128,* 8607-8614

78. Seraphine V. Wegner; Ayse Okesli; Peng Chen; and Chuan He, *J. Am. Chem. Soc.*, **2007**, *129,* 3474-3475

79. Lei Liu; Deqing Zhang; Guanxin Zhang; Junfeng Xiang; Daoben Zhu, *Org. Lett.*, **2008**, *11*, 2271-2274

80. Sung Kuk Kim; Ju Han Bok; Richard A. Bartsch; Jin Yong Lee; Jong Seung Kim, *Org. Lett.*, **2005**, *22*, 4839-4842

81. Hua Bai; Chun Li; Gaoquan Shi, *ChemPhysChem* **2008**, *9*, 1908-1913

82. Kazuhisa Fujimoto; Yu Muto; Masahiko Inouye, *Bioconjugate Chem.*, **2008**, *6*, 1132-1134

83. Hyun-Woo Rhee; Chang-Ro Lee; Seung-Hyon Cho; Mi-Ryung Song; Michael Cashel; Hyon E. Choy; Young-Jae Seok; Jong-In Hong, *J. Am. Chem. Soc.* **2008**, *130*, 784-785

84. Liping Ding; Yu Fang; G. J. Blanchard, *Langmuir* **2007**, *22*, 11042-11050

85. Akimitsu Okamoto; Yuji Ochia; Isao Saito, *Chem. Commun.* **2005**, *9*, 1128-1130

86. Boden, B. N.; Jardine, K. J.; Leung, A. C. W.; MacLachlan, M. J. *Org. Lett.* **2006**, *8*, 1855-1858

87. Shiraishi, Y.; Tokitoh, Y.; Nishimura, G.; Hirai, T. *J. Phys. Chem. B* **2007**, *111*, 5090-5100

88. Fujiwara Y.; Amao Y.; *Sens. Actuators B* **2003**, *89*, 187-191

89. Cho, H.-J.; Hwang, D.-H.; Lee, J.-I.; Jung, Y.-K.; Park, J.-H.; Lee, J.; Lee, S.-K.; Shim, H.-K. *Chem. Mater*. **2006**, *18*, 3780-3787

90. Imae, I.; Kawakami, Y.; Ooyama, Y.; Harima, Y. *Macromol. Symp.* **2007**, *249-250*, 50-55

91. Imae, I.; Kawakami, Y. *J. Mater. Chem.* **2005**, *15*, 4581

92. Xiao, Y.; Liu, L.; He, C.; Chin, W. S.; Lin, T.; Mya, K. Y.; Huang, J.; Lu, X. *J. Mater. Chem.* **2006**, 9, 829-836

93. André, P.; Cheng, G.; Ruseckas, A.; Mourik, T. V.; Früchtl, H.; Crayston, J. A.; Morris, R. E.; Cole-Hamilton, D.; Samuel, I. D. W. *J. Phys. Chem. B* **2008**, *112*, 16382-16392

94. Froehlich, J. D.; Young, R.; Nakamura, T.; Ohmori, Y.; Li, S.; Mochizuki, A. *Chem. Mater.* **2007**, *19*, 4991-4997

95. Chih-Chia Cheng; Chen-Han Chien; Ying-Chieh Yen; Yun-Sheng Ye; Fu-Hsiang Ko; Chun-Hung Lin; Feng-Chih Chang, *Acta Mater.* **2009**, *57*, 1938-1946

96. Zhang, K.; Chen, Z.; Yang, C.; Zhang, X.; Tao, Y.; Duan, L.; Chen, L.; Zhu, L.; Qin, J.; Cao, Y. *J. Mater. Chem.* **2007**, *17*, 3451

97. Zhao, W.; Cao, T.; White, J. M. *Adv. Funct. Mater.* **2004**, *14*, 783-790

98. Xiao, S.; Nguyen, M.; Gong, X.; Cao, Y.; Wu, H.; Moses, D.; Heeger, A. J. *Adv. Funct. Mater.* **2003**, *13*, 25-29

99. Miyake, J.; Chujo, Y. *Macromol. Rapid Commun.* **2008**, *29*, 86-92

100. Jong-Min Kang; Hoon-Je Cho; Jonghee Lee; Jeong-Ik Lee; Sang-Kyu Lee; Nam-Sung Cho; Do-Hoon Hwang; Hong-Ku Shim, *Macromolecules* **2006**, *39*, 4999-5008

101. Jonghee Lee; Hoon-Je Cho; Nam Sung Cho; Do-Hoon Hwang ; Jong-Min Kang; Eunhee Lim; Jeong-Ik Lee; Hong-Ku Shim, *J. Polym. Sci. Pol. Chem.* **2006**, *44*, 2943-2954

102. Miyake, J.; Chujo, Y. *J. Polym. Sci. Pol. Chem.* **2008**, *46*, 6035-6040

103. Miyake, J.; Chujo, Y. *J. Polym. Sci. Pol. Chem.* **2008**, *46*, 8112-8116

104. Lin, H. C.; Kuo, S. W.; Huang, C. F.; Chang, F. C. *Macromol. Rapid Commun.* **2006**, *27*, 537-541

105. Kuo, S. W.; Lin, H. C.; Huang, W. J.; Huang, C. F.; Chang, F. C. *J. Polym. Sci. Part B: Polym. Phys.* **2006**, *44*, 673-686

106. Feher, F. J.; Budzichowski, T. A.; Blanski, R. L.; Weller, K. J.; Ziller, J. W. *Organometallics* **1991**, *10*, 2526-2528

107. Schmid, G.; Pugin, R.; Malm, J.-O.; Bovin, J.-O. *Eur. J. Inorg. Chem.* **1998**, 813-817

108. Kim, Y. H.; Yoon, D. K.; Lee, E. H.; Ko, Y. K.; Jung, H.-T. *J. Phys. Chem. B* **2006**, *110*, 20836-20842

109. Johnson, P. C.; Offen, H. W. *J. Chem. Phys.* **1969**, *73*, 834

110. Zucolotto, V.; Faccto, A. D.; Santos, F. R.; Mendonca, C. R.; Guimaras, F. E. G.; Oliveira, O. N., Jr. *J. Phys. Chem. B,* **2005**, *109*, 7063-7066

111. Ye, K.; Wang, J.; Sun, H.; Liu, Y.; Mu, Z.; Li, F.; Jiang, S.; Zhang, J.; Zhang, H.; Wang, Y.; Che, C.-M. *J. Phys. Chem. B* **2005**, *109*, 8008-8016

112. Shigematsu, K. Crystal Growth of Alkali Salts from Concentrated Aqueous Solutions. In *Crystallization Processes*; H. Ohtaki, ed.; John Wiley and Sons, New York, 1999, *3*, 69

113. Ling Liu, Ming Tian, Wei Zhang, Liqun Zhang, James E. Mark, *polymer*, **2007**, *48*, 3201-3212

114. Hongying Li, Junying Zhang, Riwei Xu, Dingsheng Yu, *Journal of Applied Polymer Science*, **2006**, *102*, 3848-3856

115. Carroll, J. B.; Frankamp, B. L.; Rotello, V. M. *Chem. Commun.* **2002**, *17*, 1892-1893